Dual dynamic scaling in deconfined quantum criticality

Yu-Rong Shu[1] and Shuai Yin[2,*]
[1]*School of Physics and Materials Science, Guangzhou University, Guangzhou 510006, China*
[2]*School of Physics, Sun Yat-Sen University, Guangzhou 510275, China*

(Received 25 January 2022; accepted 14 March 2022; published 21 March 2022)

Emergent symmetry is one of the characteristic phenomena in deconfined quantum critical points (DQCP). As its nonequilibrium generalization, the dual dynamic scaling was recently discovered in the nonequilibrium imaginary-time relaxation dynamics in the DQCP of the J-Q_3 model. In this paper, we study the nonequilibrium imaginary-time relaxation dynamics in the J-Q_2 model, which also hosts a DQCP belonging to the same equilibrium universality class. We not only verify the universality of the dual dynamic scaling at the critical point but also investigate the breakdown and the vestige of the dual dynamic scaling when the tuning parameter is away from the critical point. We also discuss possible experimental realizations in devices of quantum computers.

DOI: 10.1103/PhysRevB.105.104420

I. INTRODUCTION

Symmetry plays pivotal roles in identifying, characterizing, and classifying phases and phase transitions in condensed-matter physics [1,2]. Traditional Landau-Ginzburg-Wilson (LGW) theory of phase transitions is based on the mechanism of spontaneous symmetry breaking, in which the symmetry of the ordered phase is always lower than that of the microscopic model [1]. In contrast, many critical systems show higher symmetry in the infrared limit than they do in the ultraviolet lattice model. For instance, space-time supersymmetry can emerge at the critical point in some topological materials [3–14]; Lorentz symmetry can emerge in the superfluid-Mott insulator quantum phase transition [15,16], critical two-subband quantum wires [17], and phase transitions in Dirac systems [18–20]; SU(3) symmetry can emerge in the critical spin-2 chain with translational invariant interaction and in the critical spin-1 chain with random bond interaction [21,22]; and extended O(N) symmetry can emerge at the multicritical point [23–26]. In two-dimensional (2D) spin systems, a prominent example in which the emergent symmetry arises as its characteristic phenomenon is the deconfined quantum critical point (DQCP) [27–29]. The DQCP was proposed as a mechanism of continuous phase transition between two spontaneous symmetry breaking phases, while the usual LGW paradigm asserts that this kind of phase transition should be first ordered [27–66]. It was shown that for the DQCP separating the antiferromagnetic (AFM) phase and valence-bond-solid (VBS) phase in SU(2)-invariant quantum magnets, SO(5) symmetry emerges to reconcile VBS and AFM order parameters [33,41,67,68]; while for the DQCP in easy-plane quantum magnets, SO(4) symmetry emerges [69].

Emergent symmetry and its breaking can induce intriguing critical properties in DQCP. For the square lattice, on the VBS side, the emergent continuous symmetry breaks down to discrete Z_4 symmetry [27–29,41]. Accordingly, the fugacity of the quadrupled coherent monopoles works as a dangerously irrelevant scaling variable, which is irrelevant exactly at the critical point, but relevant in the ordered VBS phase [70–75]. Pertinent to this variable, an extra divergent length ξ', which measures the spinon confinement length or the thickness of the VBS domain walls, develops in addition to the conventional correlation length ξ [29,50], and they satisfy $\xi' \propto \xi^{\nu'/\nu}$ with ν and ν' being the corresponding critical exponents [70–75]. It was plausibly shown that the interplay between these two length scales may take responsibility for some anomalous equilibrium scaling behaviors near the DQCP [49,50], although a very weak first-order phase transition with pseudocritical phenomena cannot be ruled out [76–85].

On the other hand, from the inflating universe to the flowing rivers, equilibrium phenomena are just the exception rather than the rule in nature. Moreover, investigations on nonequilibrium critical properties are of particular significance since universal time-dependent behaviors always appear near a critical point [86–90]. In classical systems, the theory of critical dynamics has been well established by classifications of the dynamic universality classes [86]. Recently, spurred by the remarkable experimental progresses in manipulating and detecting the nonequilibrium quantum process, the quantum critical dynamics has attracted intensive attention from both theoretical and experimental aspects [87–90]. Among these studies, it was shown that the scaling properties in the imaginary-time relaxation dynamics near quantum critical points resemble those in the classical short-time critical dynamics [91–99].

Inspired by the above intriguing issues, a natural question arises: How the emergent symmetry and the associated scaling properties with two length scales affect the nonequilibrium dynamics in DQCP. In our previous paper [100], we studied the imaginary-time relaxation dynamics at the DQCP of the J-Q_3 model. We found that with an ordered initial VBS (Néel) state, the relaxation dynamics of the VBS (Néel) order parameter is controlled by the conventional correlation length

*yinsh6@mail.sysu.edu.cn

ξ, while the dynamics of the Néel (VBS) order parameter is controlled by the confinement length ξ'. A *dual dynamic scaling*, which states that the dynamic scaling forms change to their dual partners as the initial states are changed to their dual counterpart, is then proposed. This dual dynamics scaling can be regarded as the nonequilibrium incarnation of the emergent symmetry in the equilibrium case. Given the fact that emergent symmetry is a common phenomenon in DQCP [27–29,41,67–69], it is imperative to explore the universality and robustness of the dual dynamic scaling in other models that host DQCPs.

In this paper, we study the nonequilibrium imaginary-time relaxation dynamics in the J-Q_2 model [33]. The model shares the same equilibrium universality class with the J-Q_3 model but has a weaker VBS order [39,101]. After estimating the critical point via the dynamics of the sign function of the order parameters, we study the relaxation behaviors of the Néel and VBS order parameters from different initial states at the critical point. By comparing the scaling forms for different quantities, we verify the universality of the dual dynamic scaling by showing that (i) the Néel and VBS order parameters are controlled by different length scales for different initial states and (ii) the dynamic scaling forms exchange under the exchange of the initial states, similar to the case of the J-Q_3 model. Moreover, we investigate dynamic scaling properties when the tuning parameter is away from the critical point. Strikingly, we find that in the short-time stage, the dual dynamic scaling, with a proper generalization of the dual transformation, can exist even in the presence of the off-critical-point effects, although in equilibrium the emergent symmetry fades away once the system is set away from its critical point. A possible experimental realization based on programmable quantum devices is also discussed.

The rest of the paper is organized as follows. In Sec. II, we introduce the equilibrium properties of the J-Q_2 model, the protocol of the imaginary-time relaxation dynamics and the numerical method. Then, in Sec. III, we give a brief review on the nonequilibrium dynamic scaling in the J-Q_3 model. After estimating the critical point of the J-Q_2 model via the nonequilibrium scaling in Sec. IV, we explore the dual dynamic scaling at the critical point for various initial states in Sec. V. In Sec. VI, we show the dynamic scaling behavior with the off-critical-point effects. Then we discuss the experimental realizations in Sec. VII. A summary is given in Sec. VIII.

II. MODEL AND IMAGINARY-TIME RELAXATION DYNAMICS

The Hamiltonian of the Sandvik's J-Q_2 model reads [33]

$$H = -J\sum_{\langle ij\rangle} P_{ij} - Q\sum_{\langle ijkl\rangle} P_{ij}P_{kl}, \tag{1}$$

in which $J > 0$ and $Q > 0$, $\langle ij\rangle$ and $\langle ijkl\rangle$ denote nearest neighbors and two nearest-neighbor pairs in horizontal rows or vertical columns on the square lattice, respectively, and P_{ij} denotes the spin singlet operator defined as $P_{ij} \equiv 1/4 - \mathbf{S}_i \cdot \mathbf{S}_j$ with $\mathbf{S}$ being the spin-1/2 operator. The system favors the Néel phase with a finite order parameter $\mathbf{M} \equiv \sum_r (-1)^r \mathbf{S}_r/N$ when $q \equiv J/Q > q_c$, while it favors the VBS phase with a finite $\mathbf{D}$ when $q < q_c$ [33], in which $\mathbf{D} \equiv D_x\hat{x} + D_y\hat{y}$ with $D_{x(y)} \equiv \sum_r (-1)^{r_{x(y)}} \mathbf{S}_r \cdot \mathbf{S}_{r+\hat{x}(\hat{y})}/L^d$ and $\hat{x}$ and $\hat{y}$ the unit lattice vectors in the x and y directions, respectively. These two ordered phases break different symmetries: the Néel order breaks the spin rotation symmetry, while the VBS order breaks the translation symmetry. The phase transition between them happens at $q = q_c \simeq 0.045$ [33,50,65]. According to the LGW theory, this phase transition should be first ordered [1]. However, plenty of numerical results with scrutiny demonstrate that this phase transition is a continuous one satisfying the DQCP theory [33,42,50,65]. Here we list the critical exponents of the J-Q_2 model relevant to this study. The dynamic exponent z is equal to 1 [33]. Recent works show that the anomalous dimension $\eta \simeq 0.25$ [67], leading to $2\beta/\nu \simeq 1.25$ from the scaling laws and the correlation length exponent is $\nu \simeq 0.455$ [65].

Remarkably, it was shown that an emergent SO(5) symmetry appears at the critical point of this Néel-VBS transition [32,67,68]. This symmetry is induced by the conservation of the monopole defects [102], indicating that the critical point is described by the non-compact $(2+1)$D quantum electrodynamics with deconfined spinons as its matter field [27–29]. Moreover, in the VBS phase, confined spinon-pairs are formed and the discrete Z_4 symmetry is broken [103–105]. To reconcile the emergent continuous symmetry at $q = q_c$ and the discrete symmetry for $q < q_c$, the fugacity of the monopole defects should take responsibility as a dangerously irrelevant scaling variable. Accordingly, besides the usual correlation length $\xi \propto |\delta|^{-\nu}$ with $\delta \equiv q - q_c$ the distance to the critical point, the confinement length $\xi' \propto |\delta|^{-\nu'}$ with $\nu' \simeq 0.585$ [50], measuring the averaged distance between two spinons, also plays significant roles [70–75]. It was shown that the interplay between these two characteristic scales can explain the anomalous scaling behaviors of the energy density of the domain wall and the susceptibility [50].

By replacing the second term, $-Q\sum_{\langle ijkl\rangle} P_{ij}P_{kl}$, in Eq. (1) with the interaction term with three nearest-neighbor pairs, $-Q\sum_{\langle ijklmn\rangle} P_{ij}P_{kl}P_{mn}$, one obtains the J-Q_3 model. The range of the VBS order in the J-Q_3 model is broader than that in the J-Q_2 model, since the interaction between singlets in the J-Q_3 model is stronger than that in the J-Q_2 model [39,40]. Despite this difference, it was shown that both models have continuous phase transitions supporting the DQCP theory and share the same equilibrium universality class [39,40]. Moreover, it was shown that at the DQCP both models exhibit the emergent SO(5) symmetry, while in the VBS order both models breaks the discrete Z_4 symmetry. Therefore, it is expected that they have similar scaling properties with two length scales. Actually, this was verified by comparing the finite-size scaling behaviors of the domain-wall energy in the J-Q_2 model and the J-Q_3 model [50,100]. The nonequilibrium dynamic scaling behaviors in the J-Q_3 model was studied in Ref. [100]. We will compare the nonequilibrium dynamics in the J-Q_2 model with that in the J-Q_3 model.

For the imaginary-time relaxation dynamics, the evolution of the wave function $|\psi(\tau)\rangle$ obeys the imaginary-time Schrödinger equation,

$$-\frac{\partial}{\partial\tau}|\psi(\tau)\rangle = H|\psi(\tau)\rangle, \tag{2}$$

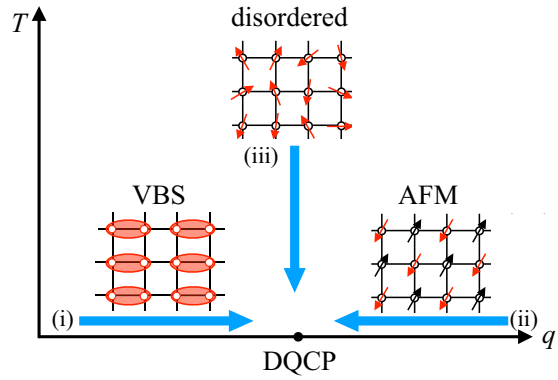

FIG. 1. Sketch of the quench dynamics in imaginary-time with different initial states. The initial states are prepared as (i) the saturated VBS state, (ii) the saturated AFM state, and (iii) the completely disordered initial state. All these states have vanishing correlation length and correspond to the fixed points of the initial states under the renormalization group transformation.

with the normalization condition $Z \equiv \langle\psi(\tau)|\psi(\tau)\rangle = 1$ [95,96]. The formal solution of the Schrödinger equation is given by

$$|\psi(\tau)\rangle = \frac{1}{\sqrt{Z}} U(\tau)|\psi(\tau_0)\rangle, \tag{3}$$

in which $U(\tau) \equiv \exp(-\tau H)$ is the imaginary-time evolution operator and τ_0 is the initial time of the evolution.

In studies of relaxation dynamics, one focuses on the dynamical scaling behaviors of different quantities from a given state [91–99]. The initial state is of key significance. In the present paper, as illustrated in Fig. 1, we will consider three kinds of uncorrelated initial states: (i) the saturated VBS state, (ii) the saturated AFM state, and (iii) the completely disordered state. All three states have vanishing correlation length and correspond to the fixed points of the initial states under the renormalization group transformation.

A wide range of quantum Monte Carlo (QMC) methods, including the stochastic series expansion, projector QMC, and world line methods, have natural connections to simulations of the imaginary-time evolution of quantum spin systems [106]. In particular, the projector QMC has proven to be a powerful tool in pursuing the imaginary-time dynamics [97,98,100,106–111]. In the projector QMC method, the imaginary-time evolution operator is Taylor expanded and the normalization can then be written as the sum of the operator sequence acting on some suitable basis states, such as the S^z basis and the valence bond basis. [101,112]. The sum over the operator sequence, along with the basis states, and the expansion power are then importance sampled. Local and global operator-loop updating schemes are developed to improve the efficiency of the Monte Carlo sampling. The expansion order is truncated to some maximum length, which is not strictly necessary in principle but brings significant convenience to implementations of the method. Note that such truncation of the expansion order causes no detectable errors. Expectation values of physical quantities are then estimated in the finial state $|\psi(\tau)\rangle$ that is propagated from $|\psi(\tau_0)\rangle$ with the sampled operator sequence and the corresponding basis states. In QMC simulations, to achieve a given initial state for the system, one needs to fix the boundaries of the imaginary-time propagation direction. Therefore, different basis are applied for convenience. For the saturated VBS state, the valence bond basis is used [101,112], while for the AFM and disordered state, the S^z basis is used [97,98,100,101,106–109,111]. For a more detailed introduction of the method, we refer to the literature [33,97,101,106–109,113].

III. BRIEF REVIEW OF THE DYNAMIC SCALING IN J-Q_3 MODEL

To study the nonequilibrium imaginary-time critical dynamics, one should first clarify the scaling relation between the imaginary-time τ and the correlation length ξ. For a usual critical point with one single divergent length scale, the scaling relation between τ and ξ satisfies $\xi \propto \tau^{1/z}$. In contrast, for the criticality with two length scales, there are two possibilities: (i) $\xi \propto \tau^{1/z}$ and $\xi' \propto \tau^{\nu'/\nu z}$ and (ii) $\xi' \propto \tau^{1/z}$ and $\xi \propto \tau^{1/z_u}$, with z_u being $z_u \equiv z\nu'/\nu$ (the subscript u means the usual correlation length). It has been shown that scenario (ii) is selected by the DQCP in the J-Q_3 model [100].

With scenario (ii), the imaginary-time dynamics for saturated ordered and completely disordered initial states should obey the scaling form

$$Y(\tau, \delta, L) = \tau^{\frac{s}{\tilde{z}}} f\left(\delta\tau^{\frac{1}{\tilde{\nu}\tilde{z}}}, \tau L^{-z}, \tau L^{-z_u}\right), \tag{4}$$

in which Y is an arbitrary operator, s is the exponent related to Y, $\delta \equiv q - q_c$ is the distance to the critical point, L is the lattice size, and $\tilde{z}$ is the dynamic exponent, which can be z or z_u, or their combination, depending on the operator Y and the dynamic process, similarly, $\tilde{\nu}$ can be ν or ν' or the combination of both, and f is the scaling function. For the three kinds of initial states introduced above, the initial state information does not appear explicitly in Eq. (4), since all of them are the fixed points of the initial states. In contrast, for other initial states with finite initial order parameters or finite initial correlations, these initial conditions should be included in the scaling form [91–99].

If $z_u = z$, Eq. (4) recovers the usual single-length-scale relaxation scaling theory, in which, for instance, at the critical point, i.e., $\delta = 0$, for a saturated initial state the order parameter scales as $M^2 = \tau^{-2\beta/\nu z_u} f(\tau L^{-z_u})$ [92,94,100], while for a disordered initial state $M^2 = L^{-d}\tau^{d/z_u - 2\beta/\nu z_u} f(\tau L^{-z_u})$ in which the factor L^{-d} stems from the random distribution of the initial state [94,100]. For both cases, in the long-time limit, the scaling forms recover the equilibrium one, namely, $M^2 \propto L^{-2\beta/\nu}$ [94,100].

In contrast, in the J-Q_3 model, a *dual dynamic scaling* appears at the critical point [100]. Specifically, from the saturated VBS initial state, D^2 is controlled by ξ and obeys the scaling form

$$D^2(\tau, L) = \tau^{-\frac{\beta}{\nu z_u}} f\left(\tau L^{-z_u}\right), \tag{5}$$

while M^2 is controlled by ξ' and obeys the scaling form

$$M^2 = L^{-d}\tau^{\frac{d}{z} - \frac{2\beta}{\nu z}} f(\tau L^{-z}). \tag{6}$$

As a dual case, from the saturated AFM initial state, M^2 is controlled by ξ and obeys the scaling form

$$M^2(\tau, L) = \tau^{-\frac{\beta}{\nu z_u}} f\left(\tau L^{-z_u}\right), \tag{7}$$

while D^2 is controlled by ξ' and obeys the scaling form

$$D^2 = L^{-d}\tau^{\frac{d}{z}-\frac{2\beta}{\nu z}} f(\tau L^{-z}). \tag{8}$$

In addition, for the disordered initial state, which is equivalent to the Néel and VBS phases, both D^2 and M^2 are controlled by ξ' and obey similar scaling forms

$$P^2 = L^{-d}\tau^{\frac{d}{z}-\frac{2\beta}{\nu z}} f(\tau L^{-z}), \tag{9}$$

in which P represents D and M. In the long-time limit, all these equations tend to the same equilibrium form, $D^2 \sim M^2 \sim L^{-2\beta/\nu}$ [33]. These scaling forms demonstrate a remarkable *dual dynamic scaling* that the dynamic scaling behaviors change to their dual partners correspondingly when the initial states turn to their dual counterpart. This dual dynamic scaling reflects the equivalence between the Néel order and the VBS order at the critical point, and can thus be regarded as the noneqilibrium generalization of the equilibrium emergent SO(5) symmetry.

IV. ESTIMATION OF THE CRITICAL POINT

In this section, we employ the nonequilibrium scaling to estimate the critical point of the J-Q_2 model Eq. (1). In equilibrium, for usual criticality with single length scale, any arbitrary dimensionless quantity A scales as $A = f(\delta L^{1/\nu})$. Accordingly, for different system sizes, curves of A versus δ will cross at the critical point if the scaling corrections are neglected. One can use this scaling feature of dimensionless quantities to estimate the critical point [106]. For the DQCP with two length scales, in general, $A = f(\delta L^{1/\tilde{\nu}})$, in which the choice of $\tilde{\nu}$ depends on the quantity. For example, when A is the Binder ratio of the order parameter, $\tilde{\nu} = \nu$; when A is the ratio of the distance between two spinons to the lattice, $\tilde{\nu} = \nu'$ [50]. Both can be employed to determine the critical point [50].

In generalizing the scaling form of A to the nonequilibrium case, according to Eq. (4), one finds that, in general, $A = f(\tau L^{-z}, \tau L^{-z_u}, \delta L^{1/\tilde{\nu}})$, in which there are two additional time-dependent variables: τL^{-z} and τL^{-z_u}. Without *a priori* wisdom, one does not know which one dominates. In the J-Q_3 model, it was found that the sign function of the VBS order parameter from the VBS initial state, $I_D \equiv \langle \mathrm{sgn}(D)\rangle$ is dominated by τL^{-z} and so does the sign function of the Néel order parameter from the AFM initial state, $I_M \equiv \langle \mathrm{sgn}(M)\rangle$ [100].

To verify the universality of the dynamic properties of $I_{D(M)}$ and determine the critical point of the J-Q_2 model, here we calculate I_D and I_M versus δ for various lattice sizes with fixed $\tau L^{-z} = 1/4$ from the VBS and the AFM initial states, respectively. Note that in principle, different values of the ratio τL^{-z} should not deliver distinguishable results of q_c as long as L is large enough.

From Fig. 2, one finds that the size dependence of the crossing points of I_D versus q for L and $2L$ decrease monotonously as L increases and converge to a point

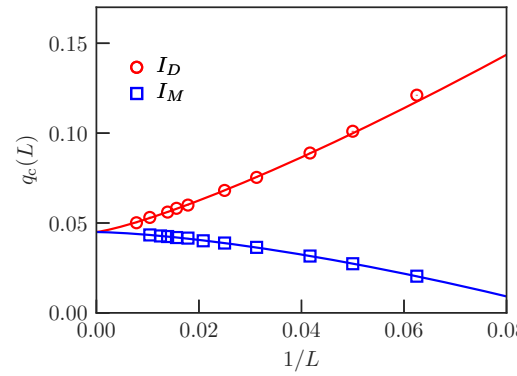

FIG. 2. Estimation of the critical point via the dynamic scaling of the sign function of the order parameter $I_{D(M)}$. The crossing points of curves of $I_{D(M)}$ versus q for L and $2L$ and fixed $\tau L^{-1} = 1/4$ converge to the critical point as $L \to \infty$, giving $q_c = 0.0449(7)$ from I_D and $q_c = 0.0453(5)$ from I_M. The solid lines indicate fits of the form $q_c(L) = q_c + aL^{-\omega}$.

$q = q_c = 0.0449(7)$ in the thermodynamic limit, which is close to the known results of the critical point [42,50,65]. Moreover, Fig. 2 also shows that the crossing points of the curves of I_M versus q for L and $2L$ increases as L increases and converge to $q = q_c = 0.0453(5)$, which is almost identical to that in the I_D case within the error bar. These results not only determine the critical point accurately, but also demonstrate that both I_D and I_M are dominated by τL^{-z} in the relaxation process from their respective ordered initial states, similar to the case of the J-Q_3 model. In the following calculations, we use $q_c = 0.045$, which is closed to the averaged value of q_c obtained by I_D and I_M.

To further examine the value of the critical point, we calculate the dynamic behavior of the spinon confinement length at $q = q_c = 0.045$. By setting the initial state as that with a triplet in the VBS background, we calculate the averaged distance between two unpaired spinons, Λ, which is proportional to the confinement length ξ' [50]. Figure 3(a) shows that in the short-time stage, $\Lambda \propto \tau^{0.953}$ with the exponent close to 1. Moreover, Fig. 3(b) shows that the rescaled curves of ΛL^{-1} versus τL^{-z} collapse onto each other well. These results not only confirm the value of the critical point, but also

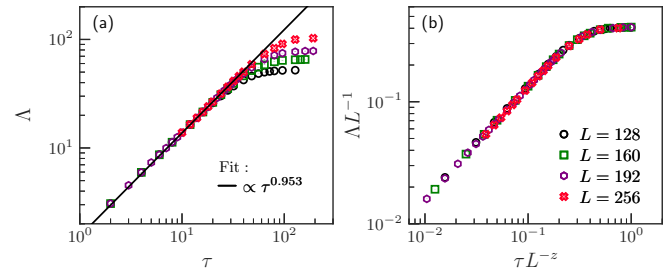

FIG. 3. Evolution of the distance between two spinons Λ at the critical point with the initial state set as the one with a triplet embedded in the VBS background. The curves for different L before and after rescaling are shown in (a) and (b), respectively. The solid line is a power-law fit that gives an exponent of 0.953, close to $1/z$. Double-logarithmic scales are used.

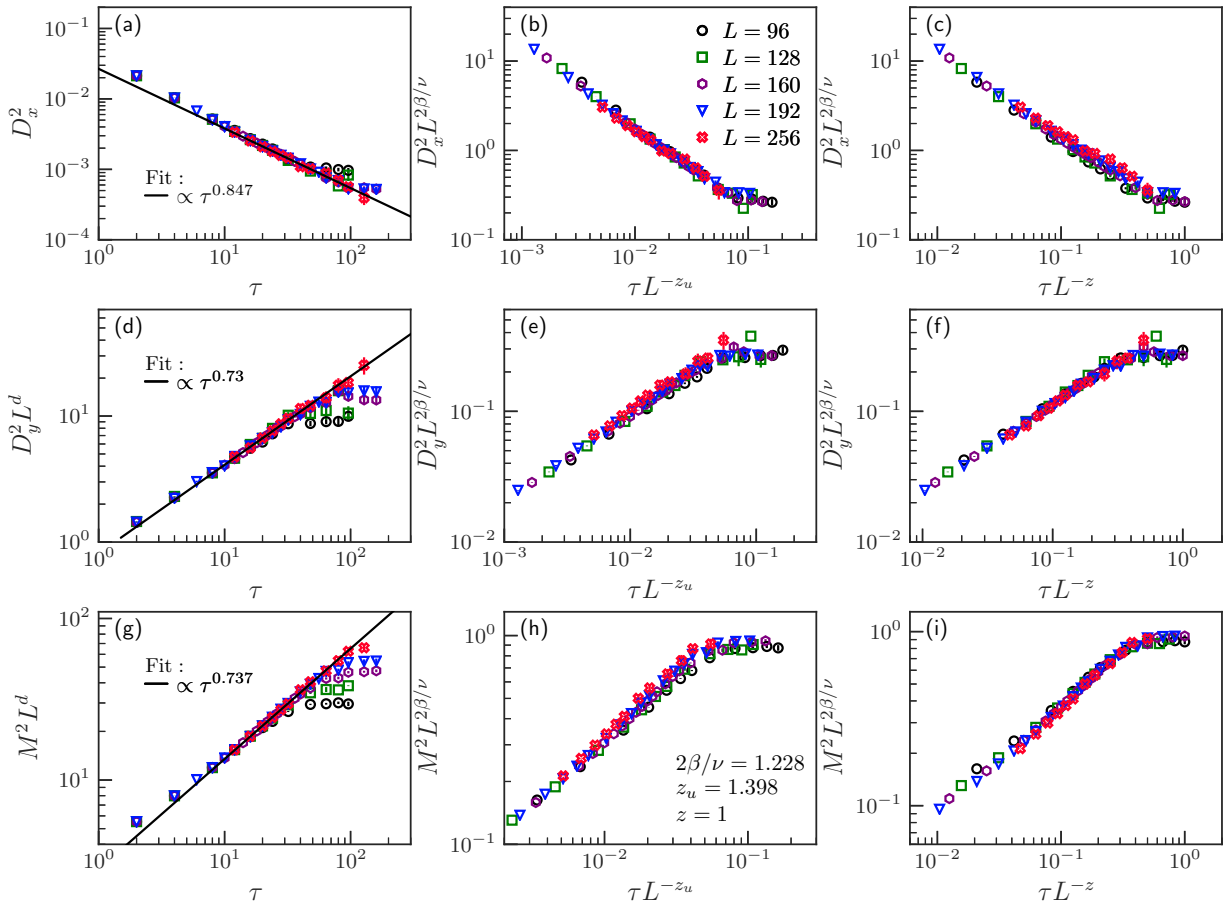

FIG. 4. Relaxation dynamics of the order parameters with the saturated VBS initial state. Evolution of D_x^2, D_y^2, and M^2 for various lattice sizes L indicated are shown in top (a)–(c), middle (d)–(f), and bottom (g)–(i) rows, respectively. In the left column (a), (d), (g), curves of the order parameter versus τ are fitted in the short-time stage by the power function. In addition, curves after rescaling are shown in the middle (b), (e), (h) and right (c), (f), (i) columns. For both columns, D_x^2, D_y^2, and M^2 are rescaled as $D_x^2 L^{2\beta/\nu}$, $D_y^2 L^{2\beta/\nu}$ and $M^2 L^{2\beta/\nu}$, respectively. To compare, τ is rescaled according to τL^{-z_u} and τL^{-z} in the middle (b), (e), (h) and right (c), (f), (i) columns, respectively. Double-logarithmic scales are used.

demonstrate that the scaling relation $\xi' \propto \tau^{1/z}$ is universal for both the J-Q_2 model and the J-Q_3 model.

However, different from the usual criticality with single length scale, in the DQCP with two length scales, not every dimensionless variable exhibits scaling properties controlled by the same scaling variable. In Sec. V A, we will show that the dynamics of the Binder ratios of the order parameters can be dominated by both τL^{-z} and τL^{-z_u}, depending on the initial states.

V. DUAL DYNAMIC SCALING AT THE CRITICAL POINT

In this section, we will explore the imaginary-time relaxation dynamics at the critical point from different initial states. We will show that the dual dynamic scaling is a universal behavior in the relaxation dynamics of the DQCP since it also appears at the critical point of the J-Q_2 model.

A. Dynamics with the VBS initial state

The VBS order breaks the Z_4 discrete symmetry. The initial VBS state is chosen as that with horizontal dimers occupying every other bond as shown in Fig. 1. Accordingly, at $\tau = 0$, D_x has a saturated value 3/8, while $D_y = 0$.

For the VBS order parameter D_x, we find from Fig. 4(a) that it relaxes according to $D_x^2 \propto \tau^{-0.847}$ in the short-time stage. This exponent is close to $2\beta/\nu z_u \simeq 0.881$ rather than $2\beta/\nu z \simeq 1.228$, in which $z_u = z\nu'/\nu \simeq 1.398$. Here, we use $\nu/\nu' \simeq 0.715$ obtained from direct fitting of the exponent ratio in Ref. [50]. Therefore, in general, the full scaling form of D_x^2 in the whole relaxation process should be $D_x^2 = \tau^{-2\beta/\nu z_u} f(\tau L^{-z_u}, \tau L^{-z})$. Moreover, previous studies showed that in equilibrium $D^2 \propto L^{-2\beta/\nu}$ [33,42]. Thus, one can infer that the full scaling form of D_x^2 should also be $D_x^2 = L^{-2\beta/\nu} g(\tau L^{-z_u}, \tau L^{-z})$, in which g is another scaling function. These two full scaling forms should be consistent with each other. This constraint indicates that the dominant scaling variable in the scaling function is τL^{-z_u} rather than τL^{-z}, so the scaling form can be converted from $D_x^2 = \tau^{-2\beta/\nu z_u} f(\tau L^{-z_u})$ to $D_x^2 = L^{-2\beta/\nu} g(\tau L^{-z_u})$ by recognizing the relation $f(\tau L^{-z_u}) = (\tau L^{-z_u})^{2\beta/\nu z_u} g(\tau L^{-z_u})$. To verify the scaling theory, in Figs. 4(b) and 4(c), we plot the rescaled curves of $D_x^2 L^{2\beta/\nu}$ versus τL^{-z_u} and compare them with those of $D_x^2 L^{2\beta/\nu}$ versus τL^{-z}. It is clear that with τ scaled with L^{-z_u},

the curves collapse better than the case with L^{-z}, indicating that it is τL^{-z_u}, or ξ, that governs the scaling form. These results show that the scaling form of D_x^2 from the VBS initial state also satisfies Eq. (5) found in the J-Q_3 model [100], confirming the universality of the scaling of D_x^2 with the horizontal VBS initial state in the Néel-VBS transition.

Note that here one may argue that D_x^2 can also be expressed as $D_x^2(\tau, L) \propto \tau^{-2\beta/\nu' z}$. In this case, $2\beta/\nu' \simeq 0.881$ is smaller than 1. Accordingly, the scaling law $2\beta/\nu' = d + z - 2 + \eta'$ gives a negative anomalous dimension η', which would imply a nonunitary theory [49,114,115]. Alternatively, to satisfy the unitarity bound of the critical point [114,115], we choose to adopt $D_x^2(\tau, L) \propto \tau^{-2\beta/\nu z_u}$, in which $2\beta/\nu$ keeps intact while an additional dynamic exponent z_u is introduced.

From the perspective of the Néel order, the saturated VBS state plays a similar role to a disordered state, since both the VBS state and the disordered state keep the spin rotation symmetry and have vanishing correlation length. For the Néel order parameter M, we find from Fig. 4(g) that it relaxes according to $M^2 \propto L^{-d}\tau^{0.737}$ in the short-time stage. The exponent 0.737 is close to $(d/z - 2\beta/\nu z) = 0.772$. Thus, the general full scaling form characterizing the whole relaxation process should be $M^2 = L^{-d}\tau^{d/z-2\beta/\nu z} f(\tau L^{-z_u}, \tau L^{-z})$. Similar to the case of D_x^2, the full scaling form can also be expressed as $M^2 = L^{-2\beta/\nu} g(\tau L^{-z_u}, \tau L^{-z})$, since in equilibrium $M^2 \propto L^{-2\beta/\nu}$. The consistency between these two full scaling forms dictates that the dominant scaling variable in the scaling function is τL^{-z} rather than τL^{-z_u}, such that the scaling form can be converted from $M^2 = L^{-d}\tau^{d/z-2\beta/\nu z} f(\tau L^{-z})$ to $M^2 = L^{-2\beta/\nu} g(\tau L^{-z})$ by recognizing the relation $f(\tau L^{-z}) = (\tau L^{-z})^{-d/z+2\beta/\nu z} g(\tau L^{-z})$. Moreover, by comparing the rescaled curves of $M^2 L^{2\beta/\nu}$ versus τL^{-z_u} and τL^{-z}, one finds from Figs. 4(h) and 4(i) that the rescaled curves collapse onto each other with τL^{-z}, while they deviate from each other with τL^{-z_u}. These results show that in the J-Q_2 model the dynamics of M^2 from the VBS initial state is controlled by the confinement length scale ξ' and satisfies Eq. (6), same as the case of the J-Q_3 model [100], confirming the universality of the dynamic critical behavior of M^2 in DQCP.

In addition, we calculate the VBS order parameter in the vertical direction D_y. From Fig. 4(d), we find that it relaxes according to $D_y^2 \propto L^{-d}\tau^{0.73}$ in the short-time stage. The exponent is close to $(d/z - 2\beta/\nu z)$, in analogy to the case of M^2. Similar analyses give that the full scaling forms should be $D_y^2 = L^{-d}\tau^{d/z-2\beta/\nu z} f(\tau L^{-z})$ and $D_y^2 = L^{-2\beta/\nu} g(\tau L^{-z})$. Moreover, by comparing the rescaled curves of $D_y^2 L^{2\beta/\nu}$ versus τL^{-z_u} and τL^{-z}, one finds that the rescaled curves collapse better with τL^{-z}, as shown in Figs. 4(e) and 4(f). From the above results, one can see that in the J-Q_2 model, with the horizontal VBS initial state, the dynamics of D_y^2 is also controlled by the confinement length scale, same as the case of M^2. Such results illustrate the equivalence under the rotation between M- and D_y-directions for the initial state with saturated D_x.

To further reveal the dynamic scaling behaviors from the VBS initial state, we also study the Binder ratios for the VBS and Néel order parameters, defined as $U_D \equiv [3 - \langle D_x^4\rangle/\langle D_x^2\rangle^2]/2$ and $U_M \equiv [3 - \langle M^4\rangle/\langle M^2\rangle^2]/2$, respectively. As dimensionless quantities, their general scaling forms are $U_{D(M)} = f_{D(M)}(\tau L^{-z_u}, \tau L^{-z})$. By comparing $U_{D(M)}$ versus τL^{-z_u} and τL^{-z} in Fig. 5, one finds that U_D is controlled by the usual length scale ξ and its dynamics obeys $U_D = f_D(\tau L^{-z_u})$, while U_M is controlled by the confinement length scale ξ' and its dynamics obeys $U_M = f_M(\tau L^{-z})$. These scaling properties are also consistent with the results that D_x^2 and M^2 are dominated by τL^{-z_u} and τL^{-z}, respectively. Combining with the scaling properties of the sign function $I_{D(M)}$, we find that in the nonequilibrium dynamics of DQCP with two length scales, dimensionless quantities can be controlled by different length scales, depending on the physical quantities themselves and the initial states applied. Moreover, our results demonstrate that special attention should be paid when one employs the short-time dynamics of the dimensionless quantities to determine the critical properties in DQCP with two length scales, although this method is often used in usual LGW phase transitions [92].

B. Dynamics with the AFM initial state

The AFM state breaks the spin SO(3) rotation symmetry. We choose the initial state as the one with saturated component in the z direction, as shown in Fig. 1.

In analogy to the situation of the Néel order with the saturated VBS initial state, from the perspective of the VBS order, the saturated AFM state plays a similar role to a disordered state, since both of them contribute zero VBS order parameters and vanishing correlation lengths. We find in Fig. 6(a) that the VBS order parameter evolves according to $D^2 \propto L^{-d}\tau^{0.73}$ in the universal short-time stage (here $D^2 \equiv D_x^2 + D_y^2$). This exponent is close to $(d/z - 2\beta/\nu z)$. By considering the equilibrium scaling $D^2 \propto L^{-2\beta/\nu}$ simultaneously [33,42], one finds that the confinement length dominates the dynamics and the scaling form of D^2 is $D^2 = L^{-d}\tau^{d/z-2\beta/\nu z} f(\tau L^{-z})$. This scaling form can be converted to $D^2 = L^{-2\beta/\nu} g(\tau L^{-z})$ by substituting $f(\tau L^{-z}) = (\tau L^{-z})^{-d/z+2\beta/\nu z} g(\tau L^{-z})$ into the former equation. Moreover, by comparing the rescaled curves of $D^2 L^{2\beta/\nu}$ versus τL^{-z_u} and τL^{-z}, as shown in Figs. 6(b) and 6(c), one finds that the rescaled curves collapse better for τL^{-z}. These results show that in the J-Q_2 model, the dynamics of D^2 from the AFM initial state is controlled by the confinement length scale and satisfies Eq. (8). These results are the same as those of the J-Q_3 model [100], confirming the universality of the dynamic critical behavior of D^2 in DQCP.

For the Néel order parameter, similar to the VBS order parameter from the saturated VBS initial state, it decays with τ as $M_z^2 \propto \tau^{-0.866}$ with the exponent close to $2\beta/\nu z_u$ as shown in Fig. 6(d). Combining with the equilibrium finite-size scaling $M_z^2 \propto L^{-2\beta/\nu}$ [33,42], one deduces that the full scaling form should be $M_z^2 = \tau^{-2\beta/\nu z_u} f(\tau L^{-z_u})$ or, equivalently, $M_z^2 = L^{-2\beta/\nu} g(\tau L^{-z_u})$. As seen in Figs. 6(e) and 6(f), by rescaling M_z^2 and τ with $L^{2\beta/\nu}$ and L^{-z_u}, respectively, we find the rescaled curves match with each other. However, when τ is rescaled with L^{-z}, the rescaled curves deviate. These results confirm that the dynamics of M_z^2 with the z-component AFM initial state is controlled by the usual correlation length scale and satisfies Eq. (7). These results are also the same as those in the J-Q_3 model [100].

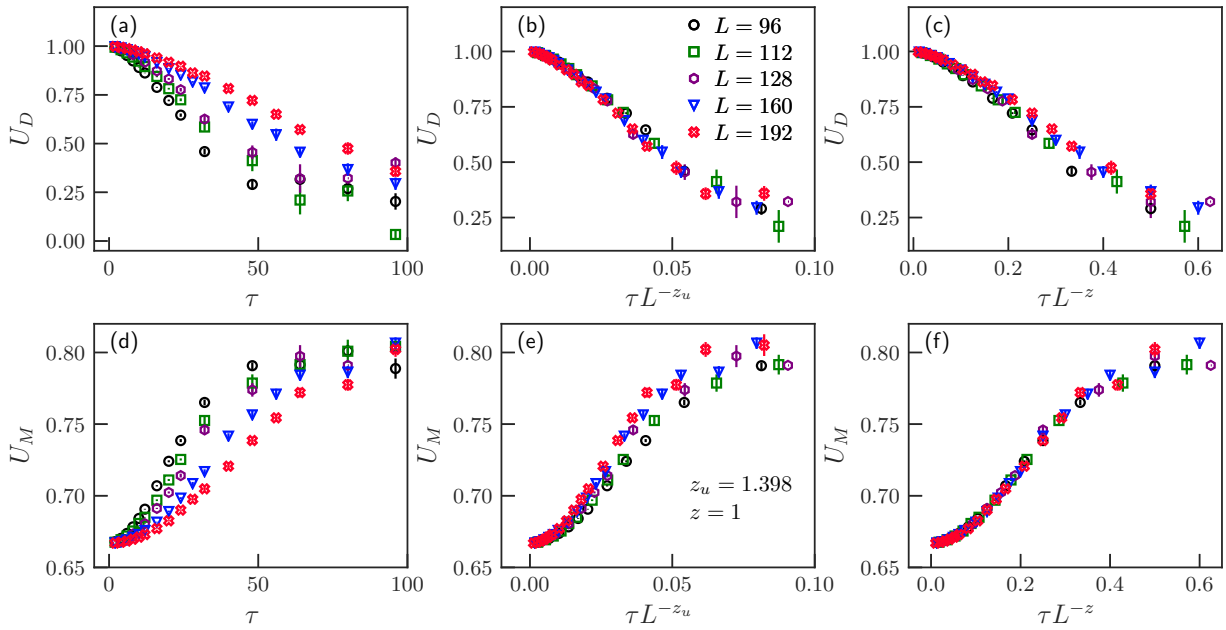

FIG. 5. Relaxation dynamics of the Binder ratios with the VBS initial state. Evolutions of U_D and U_M for various lattice sizes L indicated are shown in top (a)–(c) and bottom (d)–(f) rows, respectively. For comparison, τ is rescaled according to τL^{-z_u} in the middle column (b), (e); while τ is rescaled according to τL^{-z} in the right column (c), (f).

C. Dynamics with the disordered initial state

The disordered initial state can be prepared in the very high-temperature region. From the perspective of the disordered state, either the Néel or the VBS order looks equivalent. Accordingly, it is expected that both D^2 and M^2 should satisfy the same scaling form: $P^2 = L^{-d}\tau^{d/z-2\beta/\nu z} f(\tau L^{-z})$, in which P represents D and M. This dynamic scaling is similar to the cases of D^2 with the AFM initial state and M^2 with the VBS initial state. To verify these scaling properties, in Figs. 7(a) and 7(d), we plot the evolution of D^2 and M^2. We

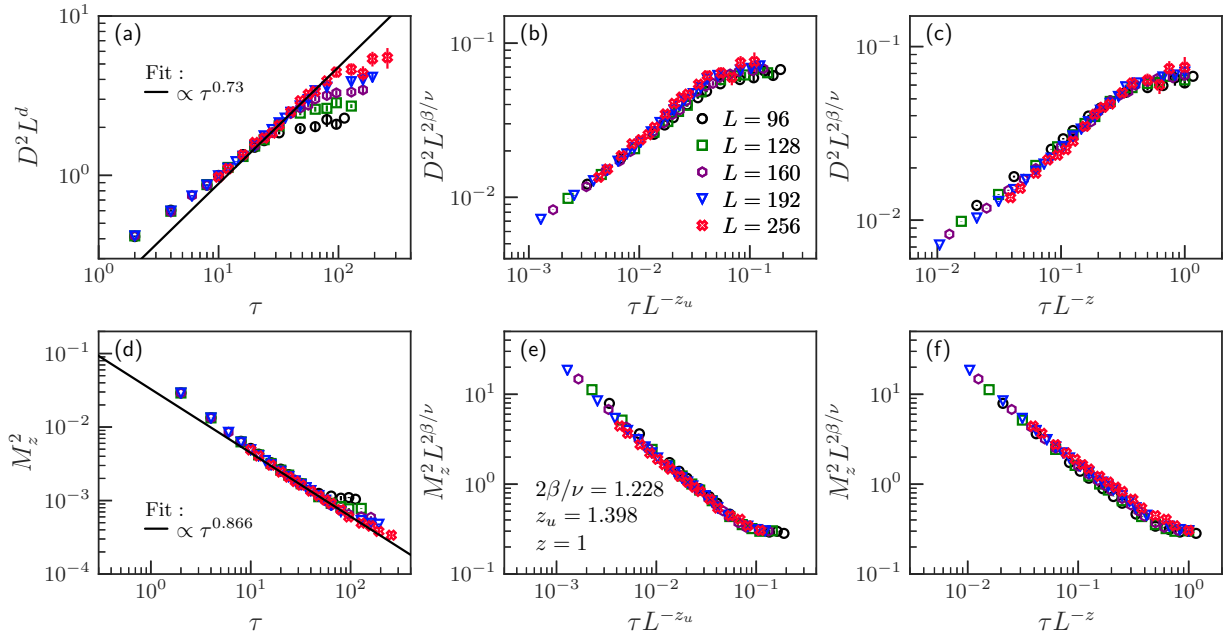

FIG. 6. Relaxation dynamics of order parameters with the AFM initial state. Evolutions of D^2 and M_z^2 for various lattice sizes L indicated are plotted in top (a)–(c) and bottom (d)–(f) rows, respectively. In the left column (a), (d), curves of the order parameter versus τ are fitted in the universal short-time stage by the power function. In addition, curves after rescaled are shown in the middle (b), (e) and right (c), (f) columns. For both columns, D^2 and M^2 is rescaled as $D^2 L^{2\beta/\nu}$ and $M_z^2 L^{2\beta/\nu}$, respectively. In contrast, τ is rescaled according to τL^{-z_u} and τL^{-z}in the middle (b), (e) and right (c), (f) columns, respectively. Double-logarithmic scales are used.

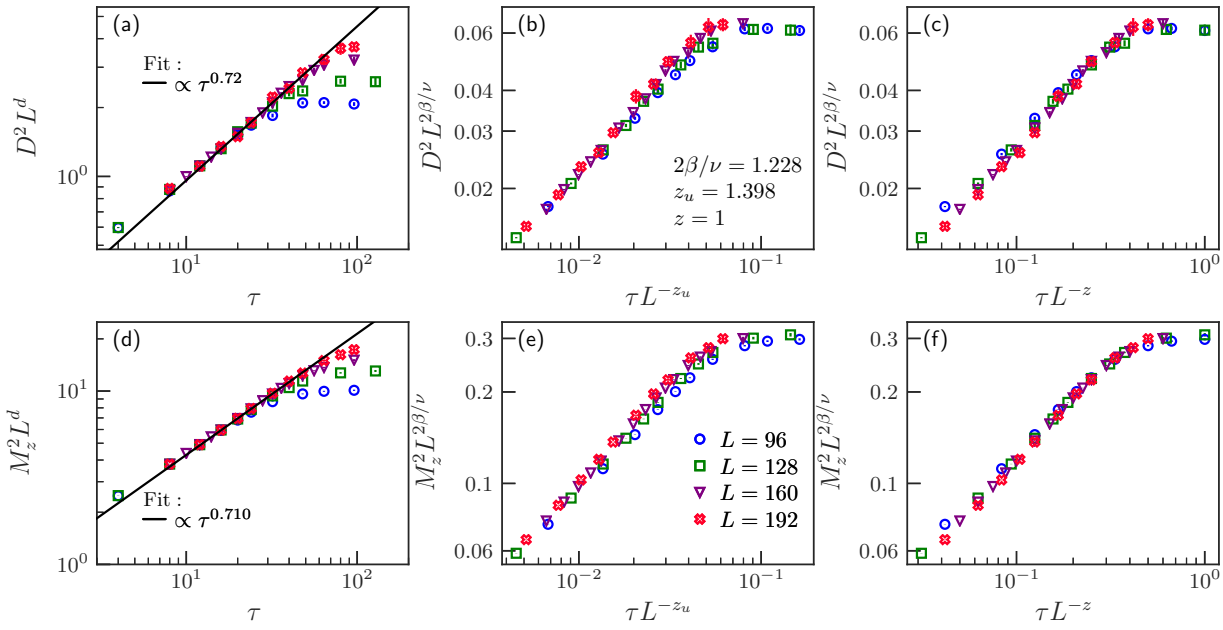

FIG. 7. Relaxation dynamics of order parameters with the disordered initial state. Evolutions of D^2 and M^2 for various lattice sizes L indicated are plotted in top (a)–(c) and bottom (d)–(f) rows, respectively. In the left column (a), (d), curves of the order parameter versus τ are fitted in the short-time stage by the power function. In addition, curves after rescaling are shown in the middle (b), (e) and right (c), (f) columns. For both columns, D^2 and M^2 is rescaled as $D^2 L^{2\beta/\nu}$ and $M_z^2 L^{2\beta/\nu}$, respectively. In contrast, τ is rescaled according to τL^{-z_u} and in the middle (b), (e) and right (c), (f) columns, respectively. Double-logarithmic scales are used.

find that in the universal short-time stage, $P^2 \propto L^{-d}\tau^{d/z-2\beta/\nu z}$. In addition, by noting that $P^2 = L^{-d}\tau^{d/z-2\beta/\nu z} f(\tau L^{-z})$ can be transformed to $P^2 = L^{-2\beta/\nu z} g(\tau L^{-z})$, we compare the curves of $P^2 L^{2\beta/\nu}$ versus τL^{-z} and τL^{-z_u}, respectively. From Figs. 7(b), 7(c), 7(e), and 7(f), one finds that with τL^{-z}, the curves collapse better, verifying the full scaling forms mentioned above. Moreover, these results demonstrate that both M^2 and D^2 are controlled by the confinement length ξ'. The same scaling properties are also found in the J-Q_3 model as shown in Eq. (9). Therefore, one concludes that these scaling properties are universal as well.

D. Dual dynamic scaling

The appearance of the emergent symmetry is a characteristic critical property of the DQCP [27,28,33,41,67–69]. For the class of the SU(2) J-Q model, the emergent symmetry at the critical point is the SO(5) symmetry, which describes the rotation symmetry between the components of the superspin $\mathcal{S} = (M_x, M_y, M_z, D_x, D_y)$, including the components of the Néel and the VBS order parameters [27,28,33,41,67,68]. The emergent symmetry is broken in both ordered phases. In particular, along with the appearance of the discrete Z_4 symmetry, scaling properties with two length scales arise on the VBS side.

In the imaginary-time relaxation dynamics, the above numerical results for the J-Q_2 model Eq. (1) show a remarkable dual dynamic scaling behavior: the scaling forms of the order parameters exchange as the initial state is rotated in the superspin space, similar to the results in the J-Q_3 model [100]. Specifically, when the initial state is rotated from the VBS state to the AFM state, the dynamic scaling form of the VBS (Néel) order parameter changes to that of the Néel (VBS) order parameter, and vice versa. Additionally, for the disordered initial state which keeps invariant under the rotation between the superspin components, both the VBS and the Néel order parameters show similar scaling behaviors. Comparing with the equilibrium emergent symmetry, we find that the dual dynamic scaling also reflects the rotation symmetry between the superspin components. Moreover, these results also show that effects induced by the interplay between two length scales are naturally included in the dual dynamic scaling.

A prominent question is why the relaxation processes of different superspin components can be governed by different length scales, albeit their equilibrium finite-size scaling forms are the same. By inspecting the relaxation behaviors under different initial conditions, one finds that for the dominant component with a saturated initial value, i.e., the component accordant with the saturated initial component, its relaxation dynamics is controlled by the usual correlation length; while for the complementary component with zero initial value, i.e., the component orthogonal to the saturated initial component, its relaxation dynamics is controlled by the confinement length. For the dominant component, the relaxation dynamics is associated with the local fluctuations whose characteristic length scale is measured by the usual correlation length ξ. For the complementary component, the average value of the component keeps zero in the relaxation process due to the symmetry of the Hamiltonian, while its average squared value in the short-time stage is proportional to L^{-d} at a given evolution time τ. Since this average squared value is directly related to the lattice size, one can infer that its dynamics is associated with the global fluctuations, which is related to the topological properties of the system. Different from the situation in the usual critical point where both the local and the

global fluctuations have the same characterized length scale ξ [94,100], in the DQCP of the J-Q model class, the global fluctuations can have a different typical length scale. To be specific, the global fluctuations correspond to the excitations with the spinons living in the vortices of the VBS domain walls and the distance between these spinons is characterized by the confinement length ξ' [29]. Accordingly, it is expected that the complementary order parameter component with a vanishing initial value should be controlled by the confinement length ξ'. This argument is also supported by the findings that with a disordered initial state, all superspin components are governed by global fluctuations, so both M^2 and D^2 are controlled by ξ'.

Besides the order parameters, other quantities can also obey the dual dynamic scaling. For instance, it is shown that the sign function $I_{D(M)}$ from the VBS (Néel) saturated initial state is controlled by the confinement length ξ'. By rotating D to M, the initial states and dynamic scaling forms change correspondingly. Note that here the scaling form for I_D and I_M are the same. Moreover, although D^2 and M^2 are controlled by the usual length scale ξ for their respective ordered initial states, their sign functions are dictated by the global flip of the order parameter over entire lattice range. Accordingly, $I_{D(M)}$ is controlled by the confinement length.

Here we discuss another intriguing puzzle on the dual dynamic scaling. According to the usual critical theory in the presence of a dangerously irrelevant scaling variable, the additional length scale ξ' only plays a role on one side of the critical point. Accordingly, asymmetric scaling properties arise between two sides of the critical point in equilibrium [75]. In the DQCP, for the relaxation dynamics from an ordered initial state to the critical point, this selected ordered state breaks the rotation symmetry in the superspin space. Therefore, the relaxation process should encode the information of the initial ordered phase during its way down to the ground state. As a result, it is expected that with different ordered initial states, asymmetric dynamic scaling should appear rather than the dual dynamic scaling, namely, following this argument, different scaling forms should be observed for the dominant order parameter on the exchange of the saturated AFM and VBS initial states. So does the complementary one. However, such prediction is inconsistent with the numerical results found here and in Ref. [100].

To solve this puzzle, we note that in equilibrium, only the ground state contributes to the expectation value and brings about the asymmetric scaling properties. In contrast, in the universal stage of nonequilibrium process, the relaxation state is the superposition of the initial state, the ground state, and the low-energy excited states. Specifically, for the AFM initial state, besides the usual spin wave excitation, excited states with quadrupled monopoles, which are directly connect to the VBS order, also play important roles at the critical point [103–105]. Although the spin-wave excitations near the AFM initial state exhibit the usual correlation length ξ, the excited states with quadrupled monopoles should be characterized by the confinement length scale ξ'. Similarly, for the VBS initial state, besides the usual spin triplet excitation, excited states with spinons staying at the vortices of the VBS domain walls that have direct connection to the Néel order, are also important at the critical point [29]. The correlation of spin-triplet excitations exhibits the usual correlation length ξ, while the excited states combining deconfined spinons and vortices of the VBS domain walls are characterized by the confinement length scale ξ'. Therefore, the relaxation state is an intertwining state of both length scales, despite the choice of ordered initial state. This argument explains the appearance of the dual dynamic scaling under the superspin rotation.

VI. DYNAMIC SCALING AWAY FROM THE CRITICAL POINT

In equilibrium, when the tuning parameter δ deviates from the critical point of the DQCP, the emergent symmetry fades away. Near the critical point, the scaling properties with two length scales also manifest themselves for finite δ [116]. For instance, it was shown that both the singlet and triplet gaps scales for $\delta^{z\nu'}$ [116]. As the nonequilibrium incarnation of the emergent symmetry, the fate of the dual dynamic scaling in the presence of a finite δ is studied in this section.

A. Off-critical-point dynamic scaling from the VBS initial state

According to Eq. (4), with the saturated horizontal VBS initial state and a small δ, D_x^2 obeys the scaling form

$$D_x^2(\tau,\delta,L)=\tau^{-\frac{\beta}{\nu z_u}}f\left(\delta\tau^{\frac{1}{\tilde{\nu}\tilde{z}}},\tau L^{-z_u}\right), \tag{10}$$

in which $\tilde{\nu}$ is ν or ν' and $\tilde{z}$ is z or z_u. However, the specific choices are unknown. To determine them, we expand the scaling function f in term of $\delta\tau^{1/\tilde{\nu}\tilde{z}}$ and obtain $\Delta D_x^2 \equiv D_x^2(\tau,\delta,L)-D_x^2(\tau,L)$ up to the leading order as

$$\Delta D_x^2(\tau,\delta)\simeq\delta\tau^{-\frac{\beta}{\nu z_u}+\frac{1}{\tilde{\nu}\tilde{z}}}. \tag{11}$$

Note that in Eq. (11), the dependence on L is ignored since in the short-time stage, ξ and ξ' are smaller than L. Similarly, $\Delta D_y^2 \equiv D_y^2(\tau,\delta,L)-D_y^2(\tau,L)$ and $\Delta M^2 \equiv M^2(\tau,\delta,L)-M^2(\tau,L)$ obey

$$\Delta D_y^2(\tau,\delta)\simeq L^{-d}\delta\tau^{\frac{d}{z}-\frac{2\beta}{\nu z}+\frac{1}{\tilde{\nu}\tilde{z}}} \tag{12}$$

and

$$\Delta M^2(\tau,\delta)\simeq L^{-d}\delta\tau^{\frac{d}{z}-\frac{2\beta}{\nu z}+\frac{1}{\tilde{\nu}\tilde{z}}}, \tag{13}$$

respectively. By analyzing the dependence of ΔD_x^2, ΔD_y^2, and ΔM^2 on τ, we can determine the specific choices of $\tilde{\nu}$ and $\tilde{z}$ for different quantities. For clarification, we enumerate the values of all possible combinations of $1/\tilde{\nu}\tilde{z}$: $1/\nu z\simeq 2.198$, $1/\nu' z=1/\nu z_u\simeq 1.572$ and $1/\nu' z_u\simeq 1.125$. In the following calculations, we choose $\delta=\pm 0.005$. We have checked that for $\delta=\pm 0.01$, there is no qualitative difference in the universal properties.

At first, we study the case for $\delta<0$ with the ground state sitting in the VBS side. From Fig. 8(a), one finds that for $\delta=-0.005$, ΔD_x^2 evolves according to $\Delta D_x^2\propto\tau^{0.34}$. This exponent is close to $-2\beta/\nu z_u+1/\nu' z_u\simeq 0.246$. The deviation between the result in Fig. 8(a) and the value 0.246 can result from finite size effect. In addition, Figs. 8(b) and 8(c) show that $\Delta D_y^2\propto\tau^{1.93}$ and $\Delta M^2\propto\tau^{1.844}$. Both their exponents are close to $d/z-2\beta/\nu z+1/\nu' z_u\simeq 1.897$. These results show that for D_x^2, D_y^2 and M^2, their off-critical-point effects in the short-time stage are all controlled by $\delta\tau^{1/\nu' z_u}$.

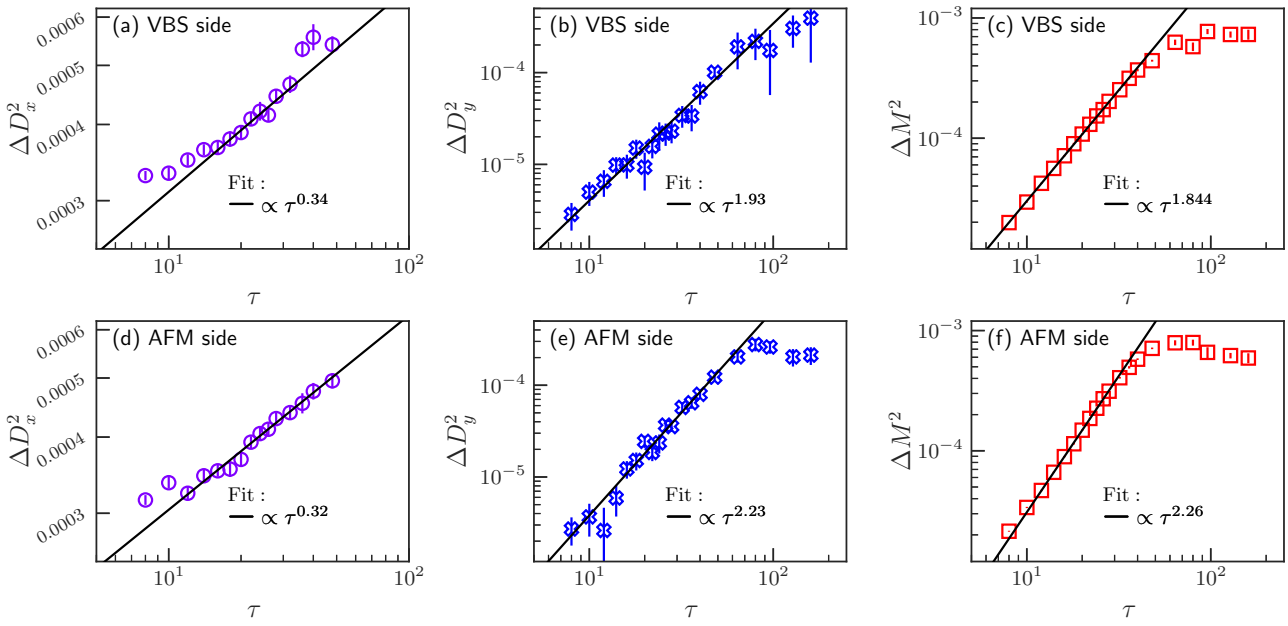

FIG. 8. Relaxation dynamics away from the critical point with the VBS initial state. Top row: For $\delta > 0$, curves of ΔD_x^2, ΔD_y^2, and ΔM^2 versus τ are plotted in (a)–(c), respectively. Bottom row: For $\delta < 0$, curves of ΔD_x^2, ΔD_y^2, and ΔM^2 versus τ are plotted in (d)–(f), respectively. Power-law fittings are implemented for all curves in the universal short-time stage. Double-logarithmic scales are used.

Since $\xi' \propto |\delta|^{-\nu'}$ and $\xi \propto \tau^{1/z_u}$, the term $\delta\tau^{1/\nu' z_u}$ combines the two arguments and reflects an effect induced by the interplay of two length scales.

Then, let us turn to the case for $\delta > 0$, in which the system is relaxed from the VBS initial state to a AFM ground state. From Fig. 8(d), one finds that for $\delta = 0.005$, ΔD_x^2 evolves according to $\Delta D_x^2 \propto \tau^{0.32}$. This exponent is close to $-2\beta/\nu z_u + 1/\nu' z_u \simeq 0.246$, similar to the case for $\delta < 0$. In contrast, for ΔD_y^2 and ΔM^2, we find that $\Delta D_y^2 \propto \tau^{2.23}$ and $\Delta M^2 \propto \tau^{2.26}$, as shown in Figs. 8(e) and 8(f). Both exponents are close to $d/z - 2\beta/\nu z + 1/\nu z_u$ or $d/z - 2\beta/\nu z + 1/\nu' z$, which are close to 2.344. These results show that for $\delta > 0$, the off-critical-point effects for ΔD_x^2, ΔD_y^2 and ΔM^2 are controlled by different scaling variables: $\delta\tau^{1/\nu' z_u}$ dominates in ΔD_x^2, while $\delta\tau^{1/\nu z_u}$ or $\delta\tau^{1/\nu' z}$ dominates in ΔD_y^2 and ΔM^2.

In addition, for ΔD_y^2 and ΔM^2, from the present numerical results, one cannot clarify which one of $\delta\tau^{1/\nu z_u}$ and $\delta\tau^{1/\nu' z}$ dominates the scaling form for $\delta > 0$. Here we argue that both should be taken into account in the short-time stage. For the former, both $\delta^{-\nu}$ and τ^{1/z_u} are related to the usual length scale ξ, and $\delta\tau^{1/\nu z_u}$ represents the ratio between the contributions from δ and τ to ξ; while for the latter, both $\delta^{-\nu'}$ and $\tau^{1/z}$ are related to the confinement length ξ', and $\delta\tau^{1/\nu' z}$ represents the ratio between the contributions from δ and τ to ξ'. These ratios can have similar order of magnitude in the universal short-time stage for finite δ. However, in the long-time stage, $\delta\tau^{1/\nu z_u}$ should dominate due to the asymmetric appearance of the dangerously irrelevant scaling variable. In the equilibrium situation, the dangerously irrelevant scaling variable only appear on the VBS side, causing anomalous scaling behaviors induced by the interplay of the usual length scale ξ and the additional confinement length scale ξ'. Therefore, in the long time limit, for $\delta > 0$, only the usual length scale, namely, $\delta\tau^{1/\nu z_u}$, should govern the scaling form.

Thus, we conclude the choice of $1/\tilde{\nu}\tilde{z}$ for different cases:

(i) When $\delta < 0$, for ΔD_x^2, ΔD_y^2, and ΔM^2, $1/\tilde{\nu}\tilde{z}$ should be $1/\nu' z_u$, which reflects the interplay of two length scales.

(ii) When $\delta > 0$, for ΔD_x^2, $1/\tilde{\nu}\tilde{z}$ is $1/\nu' z_u$ as well, while for ΔD_y^2 and ΔM^2, $1/\tilde{\nu}\tilde{z}$ can be $1/\nu z_u$ or $1/\nu' z$ in the short-time stage, while $1/\tilde{\nu}\tilde{z}$ should be $1/\nu z_u$ in the long-time stage.

B. Off-critical-point dynamic scaling from the AFM initial state

From the saturated AFM initial state, similar analyses give that for a small δ, in the universal short-time stage, ΔD^2 obeys the following scaling relation:

$$\Delta D^2(\tau, \delta) \simeq L^{-d}\delta\tau^{\frac{d}{z}-\frac{2\beta}{\nu z}+\frac{1}{\tilde{\nu}\tilde{z}}}, \tag{14}$$

and ΔM_z^2 obeys

$$\Delta M_z^2(\tau, \delta) \simeq \delta\tau^{-\frac{2\beta}{\nu z_u}+\frac{1}{\tilde{\nu}\tilde{z}}} \tag{15}$$

to the leading order of $\delta\tau^{1/\tilde{\nu}\tilde{z}}$.

First, we study the case for $\delta < 0$ with the ground state sitting in the VBS side. From Fig. 9(a), one finds that for $\delta = -0.005$, ΔM_z^2 evolves according to $\Delta M_z^2 \propto \tau^{0.36}$. This exponent is close to $-2\beta/\nu z_u + 1/\nu' z_u \simeq 0.246$, similar to the scaling relation of ΔD_x^2 from the VBS initial state. In contrast, from Fig. 9(b), we find that $\Delta D^2 \propto \tau^{2.47}$ with its exponent close to $d/z - 2\beta/\nu z + 1/\nu z_u$ and $d/z - 2\beta/\nu z + 1/\nu' z$, both close to 2.344. Similar to the case of ΔM^2 with $\delta > 0$ from the VBS initial state, we argue that both $\delta\tau^{1/\nu z_u}$ and $\delta\tau^{1/\nu' z}$ should be taken into account in the universal short-time stage. However, in the long-time stage, different from the case when the system is relaxed from the saturated VBS initial state to the AFM side, from the saturated AFM initial state to the VBS side, besides $\delta\tau^{1/\nu z_u}$, $\delta\tau^{1/\nu' z}$ should also play important roles.

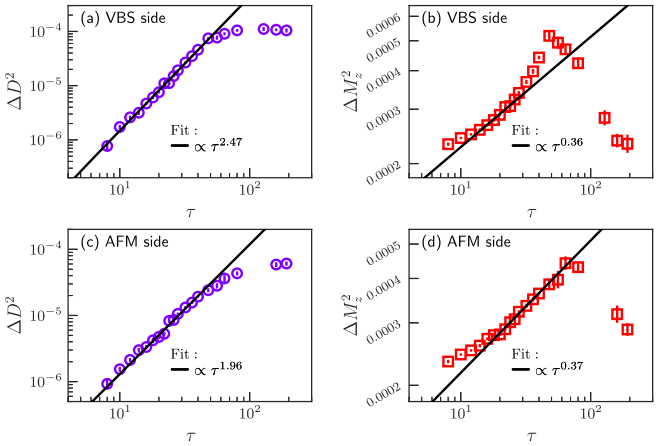

FIG. 9. Relaxation dynamics away from the critical point with the AFM initial state. Top row: For $\delta > 0$, curves of ΔD^2 and ΔM_z^2 versus τ are plotted in (a) and (b), respectively. Bottom row: For $\delta < 0$, curves of ΔD^2 and ΔM_z^2 versus τ are plotted in (c) and (d), respectively. Power-law fittings are implemented for all curves in the universal short-time stage. Double-logarithmic scales are used.

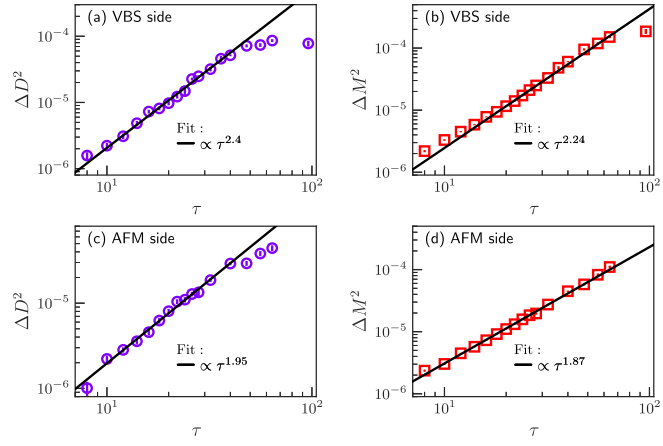

FIG. 10. Relaxation dynamics away from the critical point with the disordered initial state. Top row: For $\delta > 0$, curves of ΔD^2 and ΔM^2 versus τ are plotted in (a) and (b), respectively. Bottom row: For $\delta < 0$, curves of ΔD^2 and ΔM^2 versus τ are plotted in (c) and (d), respectively. Power-law fittings are implemented for all curves in the universal short-time stage. Double-logarithmic scales are used.

Then, we turn to the case for $\delta > 0$ and the ground state is in the Néel phase. From Fig. 9(c), one finds that for $\delta = 0.005$, ΔM_z^2 evolves according to $\Delta M_z^2 \propto \tau^{0.37}$. This exponent is close to $-2\beta/\nu z_u + 1/\nu' z_u \simeq 0.246$, similar to previous scaling relation of ΔM_z^2 for $\delta < 0$. Moreover, Fig. 9(d) shows that $\Delta D^2 \propto \tau^{1.97}$ with the exponent close to $d/z - 2\beta/\nu z + 1/\nu' z_u \simeq 1.897$. These results show that for ΔD^2 and ΔM_z^2, the off-critical-point effects in the universal short-time stage is controlled by $\delta\tau^{1/\nu' z_u}$ when $\delta > 0$.

Thus, we conclude the choice of $1/\tilde{\nu}\tilde{z}$ for different cases:

(i) When $\delta < 0$, for ΔM_z^2, $1/\tilde{\nu}\tilde{z}$ is $1/\nu' z_u$ while for ΔD^2, $1/\tilde{\nu}\tilde{z}$ can be $1/\nu z_u$ or $1/\nu' z$.

(ii) When $\delta > 0$, for ΔM_z^2 and ΔD^2, $1/\tilde{\nu}\tilde{z}$ should be $1/\nu' z_u$.

C. Off-critical-point dynamic scaling from the disordered initial state

For the disordered initial state, similar analyses give that for a small δ, in the universal short-time stage, ΔD^2 obeys

$$\Delta D^2(\tau, \delta) \simeq L^{-d}\delta\tau^{\frac{d}{z}-\frac{2\beta}{\nu z}+\frac{1}{\tilde{\nu}\tilde{z}}} \tag{16}$$

and ΔM^2 obeys

$$\Delta M^2(\tau, \delta) \simeq L^{-d}\delta\tau^{\frac{d}{z}-\frac{2\beta}{\nu z}+\frac{1}{\tilde{\nu}\tilde{z}}} \tag{17}$$

to the leading order of $\delta\tau^{1/\tilde{\nu}\tilde{z}}$.

For $\delta < 0$ with the VBS ground state, Figs. 10(a) and 10(b) shows that for $\delta = -0.005$, ΔD^2 and ΔM^2 evolve according to $\Delta D^2 \propto \tau^{2.4}$ and $\Delta M^2 \propto \tau^{2.24}$, respectively. The two exponents are close to $d/z - 2\beta/\nu z + 1/\nu z_u$ and $d/z - 2\beta/\nu z + 1/\nu' z$, both close to 2.344. As discussed above, both $\delta\tau^{1/\nu z_u}$ and $\delta\tau^{1/\nu' z}$ should make contributions in the short-time regime. For $\delta > 0$ with the AFM ground state, from Figs. 10(c) and 10(d), one finds that $\Delta D^2 \propto \tau^{1.95}$ and $\Delta M^2 \propto \tau^{1.87}$ when $\delta = 0.005$. Both these exponents are close to $d/z - 2\beta/\nu z + 1/\nu' z_u = 1.897$, demonstrating the off-critical-point effects are mainly contributed by $\delta\tau^{1/\nu' z_u}$.

Thus, we conclude that with the disordered initial state,

(i) When $\delta < 0$, for both ΔM^2 and ΔD^2, $1/\tilde{\nu}\tilde{z}$ can be $1/\nu z_u$ or $1/\nu' z$.

(ii) When $\delta > 0$, for both ΔM^2 and ΔD^2, $1/\tilde{\nu}\tilde{z}$ is $1/\nu' z_u$.

D. Breakdown and vestige of the dual dynamic scaling

From the above results, we find that the dual dynamic scaling breaks down under the rotation between the superspin components when the tuning parameter is away from its critical point. In the long-time limit, the system reaches its equilibrium ground state, in which the asymmetric scaling properties between the Néel order and the VBS order appear [71,75] and meanwhile the emergent symmetry fades out [41]. In the short-time stage, from the ordered initial state, for a fixed $\delta \neq 0$, under the rotation between D and M, one finds that the dual dynamic scaling also breaks down. Although the dominant order parameters of the ordered initial states obey similar scaling behavior, the complementary order parameters behave quite differently. When relaxed from the saturated VBS initial state to the VBS side, i.e., $\delta < 0$, for the complementary order parameter M, its off-critical-point effect ΔM^2 is dominated by $\delta\tau^{d/z-2\beta/\nu z+1/\nu' z_u}$; as the dual case, from the AFM initial state, in contrast, for the complementary order parameter D, its off-critical-point effect ΔD^2 is dominated by $\delta\tau^{d/z-2\beta/\nu z+1/\nu' z}$ and/or $\delta\tau^{d/z-2\beta/\nu z+1/\nu z_u}$. Similarly, when relaxed from the saturated VBS initial state to the AFM side, i.e., $\delta > 0$, ΔM^2 is dominated by $\delta\tau^{d/z-2\beta/\nu z+1/\nu' z}$ and/or $\delta\tau^{d/z-2\beta/\nu z+1/\nu z_u}$; as its dual case, from the AFM initial state, in contrast, ΔD^2 is dominated by $\delta\tau^{d/z-2\beta/\nu z+1/\nu' z}$. This demonstrates that the dual dynamic scaling breaks when the parameter is tuned away from the critical point.

However, strikingly, for the ordered initial states, we find that the dual dynamic scaling in the universal short-time stage can restore once the transformations $M \Leftrightarrow D$ and $\delta \Leftrightarrow -\delta$ are simultaneously implemented. Under this joint transformation, the relaxation dynamics of the VBS (Néel) order parameter for $\delta < 0$ with the VBS initial state can be dualized to the relaxation dynamics of the Néel (VBS) order parameter for

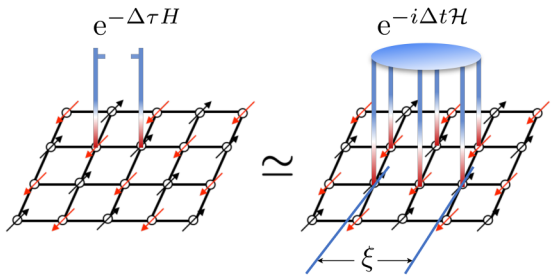

FIG. 11. Realization of imaginary-time relaxation dynamics via unitary quantum gates.

$\delta > 0$ with the Néel initial state and vice versa. Accordingly, the scaling behaviors of both the dominant and complementary order parameters keep invariant under this joint dual transformation. In this sense, the dual dynamic scaling is maintained.

The vestige of the dual dynamic scaling in the short-time stage demonstrates that the nonequilibrium dynamics can even exhibit much higher symmetry than the equilibrium state. Therefore, unlike the fade of the emergent symmetry on running away from the critical point in equilibrium, the dual dynamic scaling can survive up to some finite δ under the joint dual transformation. A possible reason is that the nonequilibrium dynamics mixes various elements together to form a state which is covariant under the dual transformation, although each single element is asymmetric under the same condition. For instance, relaxing from the saturated VBS initial state to the VBS side with a finite $\delta < 0$, the relaxation dynamics mixes the VBS background, the VBS ground state, and the topological defects with spinons living at the vortices of the VBS domain walls; while relaxing from the AFM initial state to the AFM side with a finite $\delta > 0$, the relaxation dynamics mixes the local fluctuations with the background in the AFM pattern, the AFM ground state, and the topological defects with quadrupled monopole excitations. The interplay between these elements may give rise to the dual dynamic scaling. However, from the disordered initial states, in the short-time stage, only global fluctuations contribute to M^2 and D^2. Thus the dual dynamic scaling in the short-time stage still exists for the transformation of $M \Leftrightarrow D$. However, it breaks down when $\delta \Leftrightarrow -\delta$ is added simultaneously, since in this case, the ground-state information, which breaks the emergent symmetry of the superspin rotation, should be simultaneously included.

VII. POSSIBLE EXPERIMENTAL REALIZATION

Recently, it was shown that quantum computers have become a vivifying platform to realizing various experiments ranging from high-energy physics [117,118] to condensed matter physics [119,120]. In particular, nonequilibrium quantum critical dynamics has been observed in D-wave devices [121] and the noisy intermediate-scale quantum device based on the Rigetti superconducting quantum chip [122]. Moreover, imaginary-time relaxation was also implemented in the various devices as a promising approach to find the ground state [123]. As illustrated in Fig. 11, imaginary-time evolution in a small time interval $\Delta\tau$ with the Hamiltonian H can be approximated by the real-time unitary evolution with the auxiliary Hamiltonian $\mathcal{H}$. By minimizing the following residual form:

$$\text{Res} \equiv \left\| \frac{e^{-\Delta\tau H}|\psi\rangle}{\langle\psi|e^{-2\Delta\tau H}|\psi\rangle} - e^{-i\Delta t\mathcal{H}}|\psi\rangle \right\|^2, \tag{18}$$

one can determine $\mathcal{H}$ [123,124]. It was shown that the interaction range in $\mathcal{H}$ is only required to have the same order of magnitude as the correlation length ξ. For our present case, the initial state is set as the uncorrelated state with vanishing correlation length [123]. Thus, it is promising that our results can be detected in these systems in the future.

VIII. SUMMARY

In summary, we have studied the nonequilibrium imaginary-time dynamics of the DQCP in the 2D J-Q_2 model. At the critical point, we have generalized the emergent symmetry in equilibrium to the dual dynamic scaling in the relaxation process. In particular, we have found that in the relaxation dynamics from the ordered initial states, although the dominant and the complementary order parameters are controlled by different length scales, they can be dualized to each other under the rotation transformation in the superspin space. In addition, we have shown that for the disordered initial state the dual dynamic scaling dictates that both the Néel and the VBS order parameter obey the same scaling form. By comparing the results of the J-Q_3 model [100], we have confirmed that the dual dynamic scaling is a universal nonequilibrium phenomenon in the DQCP that separates the Néel order and the VBS order. Furthermore, we have studied the relaxation dynamics away from the critical point and found that the dual dynamic scaling can even exist when the emergent symmetry in the ground state has been broken. We have attributed the appearance of the dual dynamic scaling at and near the DQCP to the superposition of information included in the initial state, ground state, and low-energy excited states. In addition, we have discussed the possible experimental realizations in fast-developing programmable quantum devices.

In this paper, we have only focused on the situation where the initial state is at its fixed points and the initial condition is absent in the scaling form. In a usual critical point with a single length scale, it was shown that the general initial state can induce interesting scaling behaviors [91,93,95–98]. In particular, in our previous paper [100], we have shown that in DQCP, the critical initial slip exponent is negative, while in usual phase transitions, this exponent is positive. Thus it is instructive to explore more general effects induced by different initial states.

Moreover, at present, direct attacks on the nonequilibrium dynamics in 2D quantum systems are still confronted with severe difficulties. Although the direct analytic continuations seem inadequate to obtain the results of the real-time dynamics, it has been shown that some universal behaviors are shared in both imaginary-time and real-time

dynamics [107,108,125,126]. In addition, it was shown that the real-time relaxation has similar scaling relations with the imaginary-time relaxation, but with different critical exponent [127–135]. Therefore, it is expected that our present paper should provide profound insights to the real-time dynamics of the DQCP.

ACKNOWLEDGMENTS

Y.R.S. acknowledges support from the National Natural Science Foundation of China (Grants No. 11947035 and No. 12104109), the Science and Technology Projects in Guangzhou (No. 202102020933). S.Y. is supported by the National Natural Science Foundation of China (Grant No. 12075324).

[1] L. D. Landau, E. M. Lifshitz, and E. M. Pitaevskii, *Statistical Physics* (Butterworth-Heinemann, New York, 1999).
[2] S. Sachdev, *Quantum Phase Transitions*, 2nd ed. (Cambridge University Press, Cambridge, 2011).
[3] S.-S. Lee, Emergence of supersymmetry at a critical point of a lattice model, Phys. Rev. B **76**, 075103 (2007).
[4] T. Grover, D. N. Sheng, and A. Vishwanath, Emergent space-time supersymmetry at the boundary of a topological phase, Science **344**, 280 (2014).
[5] S.-K. Jian, Y.-F. Jiang, and H. Yao, Emergent Spacetime Supersymmetry in 3D Weyl Semimetals and 2D Dirac Semimetals, Phys. Rev. Lett. **114**, 237001 (2015).
[6] L. Huijse, B. Bauer, and E. Berg, Emergent Supersymmetry at the Ising–Berezinskii-Kosterlitz-Thouless Multicritical Point, Phys. Rev. Lett. **114**, 090404 (2015).
[7] A. Rahmani, X. Zhu, M. Franz, and I. Affleck, Emergent Supersymmetry from Strongly Interacting Majorana Zero Modes, Phys. Rev. Lett. **115**, 166401 (2015).
[8] W. Witczak-Krempa and J. Maciejko, Optical Conductivity of Topological Surface States with Emergent Supersymmetry, Phys. Rev. Lett. **116**, 100402 (2016).
[9] Z.-X. Li, Y.-F. Jiang, and H. Yao, Edge Quantum Criticality and Emergent Supersymmetry in Topological Phases, Phys. Rev. Lett. **119**, 107202 (2017).
[10] S.-K. Jian, C.-H. Lin, J. Maciejko, and H. Yao, Emergence of Supersymmetric Quantum Electrodynamics, Phys. Rev. Lett. **118**, 166802 (2017).
[11] E. O'Brien and P. Fendley, Lattice Supersymmetry and Order-Disorder Coexistence in the Tricritical Ising Model, Phys. Rev. Lett. **120**, 206403 (2018).
[12] J. Yu, R. Roiban, S.-K. Jian, and C.-X. Liu, Finite-scale emergence of $2+1$D supersymmetry at first-order quantum phase transition, Phys. Rev. B **100**, 075153 (2019).
[13] S. Yin and Z.-Y. Zuo, Fermion-induced quantum critical point in the Landau-Devonshire model, Phys. Rev. B **101**, 155136 (2020).
[14] S. E. Han, J. Lee, and E. G. Moon, Lattice vibration as a knob on exotic quantum criticality, Phys. Rev. B **103**, 014435 (2021).
[15] L. Pollet and N. Prokof'ev, Higgs Mode in a Two-Dimensional Superfluid, Phys. Rev. Lett. **109**, 010401 (2012).
[16] K. Chen, L. Liu, Y. Deng, L. Pollet, and N. Prokof'ev, Universal Properties of the Higgs Resonance in $(2+1)$-Dimensional U(1) Critical Systems, Phys. Rev. Lett. **110**, 170403 (2013).
[17] M. Sitte, A. Rosch, J. S. Meyer, K. A. Matveev, and M. Garst, Emergent Lorentz Symmetry with Vanishing Velocity in a Critical Two-Subband Quantum Wire, Phys. Rev. Lett. **102**, 176404 (2009).
[18] Z.-X. Li, Y.-F. Jiang, S.-K. Jian, and H. Yao, Fermion-induced quantum critical points, Nat. Commun. **8**, 314 (2017).
[19] B. Roy, V. Juričić, and I. F. Herbut, Emergent Lorentz symmetry near fermionic quantum critical points in two and three dimensions, J. High Energy Phys. 04 (2016) 018.
[20] E. Torres, L. Classen, I. F. Herbut, and M. M. Scherer, Fermion-induced quantum criticality with two length scales in Dirac systems, Phys. Rev. B **97**, 125137 (2018).
[21] P. Chen, Z.-L. Xue, I. P. McCulloch, M.-C. Chung, C.-C. Huang, and S.-K. Yip, Quantum Critical Spin-2 Chain with Emergent SU(3) Symmetry, Phys. Rev. Lett. **114**, 145301 (2015).
[22] V. L. Quito, J. A. Hoyos, and E. Miranda, Emergent SU(3) Symmetry in Random Spin-1 Chains, Phys. Rev. Lett. **115**, 167201 (2015).
[23] P. Calabrese, A. Pelissetto, and E. Vicari, Multicritical phenomena in $O(n_1)\bigoplus O(n_2)$-symmetric theories, Phys. Rev. B **67**, 054505 (2003).
[24] L. Janssen, I. F. Herbut, and M. M. Scherer, Compatible orders and fermion-induced emergent symmetry in Dirac systems, Phys. Rev. B **97**, 041117(R) (2018).
[25] B. Roy, P. Goswami, and V. Juričić, Itinerant quantum multicriticality of two-dimensional Dirac fermions, Phys. Rev. B **97**, 205117 (2018).
[26] E. Torres, L. Weber, L. Janssen, S. Wessel, and M. M. Scherer, Emergent symmetries and coexisting orders in Dirac fermion systems, Phys. Rev. Res. **2**, 022005(R) (2020).
[27] T. Senthil, A. Vishwanath, L. Balents, S. Sachdev, and M. P. A. Fisher, Deconfined quantum critical points, Science **303**, 1490 (2004).
[28] T. Senthil, L. Balents, S. Sachdev, A. Vishwanath, and M. P. A. Fisher, Quantum criticality beyond the Landau-Ginzburg-Wilson paradigm, Phys. Rev. B **70**, 144407 (2004).
[29] M. Levin and T. Senthil, Deconfined quantum criticality and Néel order via dimer disorder, Phys. Rev. B **70**, 220403(R) (2004).
[30] A. Tanaka and X. Hu, Many-Body Spin Berry Phases Emerging from the π-Flux State: Competition between Antiferromagnetism and the Valence-Bond-Solid State, Phys. Rev. Lett. **95**, 036402 (2005).
[31] F. S. Nogueira and H. Kleinert, Quantum Electrodynamics in $2+1$ Dimensions, Confinement, and the Stability of $U(1)$ Spin Liquids, Phys. Rev. Lett. **95**, 176406 (2005).
[32] T. Senthil and M. P. A. Fisher, Competing orders, nonlinear sigma models, and topological terms in quantum magnets, Phys. Rev. B **74**, 064405 (2006).
[33] A. W. Sandvik, Evidence for Deconfined Quantum Criticality in a Two-Dimensional Heisenberg Model with Four-Spin Interactions, Phys. Rev. Lett. **98**, 227202 (2007).

[34] F. S. Nogueira, S. Kragset, and A. Sudbø, Quantum critical scaling behavior of deconfined spinons, Phys. Rev. B **76**, 220403(R) (2007).

[35] R. K. Kaul and R. G. Melko, Large-N estimates of universal amplitudes of the $\mathbb{C}\mathbb{P}^{N-1}$ theory and comparison with a $S = \frac{1}{2}$ square-lattice model with competing four-spin interactions, Phys. Rev. B **78**, 014417 (2008).

[36] R. G. Melko and R. K. Kaul, Scaling in the Fan of an Unconventional Quantum Critical Point, Phys. Rev. Lett. **100**, 017203 (2008).

[37] A. Gellé, A. M. Läuchli, B. Kumar, and F. Mila, Two-dimensional quantum antiferromagnet with a fourfold degenerate dimer ground state, Phys. Rev. B **77**, 014419 (2008).

[38] F. S. Nogueira and H. Kleinert, Compact quantum electrodynamics in $2+1$ dimensions and spinon deconfinement: A renormalization group analysis, Phys. Rev. B **77**, 045107 (2008).

[39] J. Lou, A. W. Sandvik, and N. Kawashima, Antiferromagnetic to valence-bond-solid transitions in two-dimensional SU(N) Heisenberg models with multispin interactions, Phys. Rev. B **80**, 180414(R) (2009).

[40] A. W. Sandvik, Finite-size scaling and boundary effects in two-dimensional valence-bond solids, Phys. Rev. B **85**, 134407 (2012).

[41] J. Lou and A. W. Sandvik, Z_4 to U(1) crossover of the order-parameter symmetry in a two-dimensional valence-bond solid, Phys. Rev. B **80**, 212406 (2009).

[42] A. W. Sandvik, Continuous Quantum Phase Transition between an Antiferromagnet and a Valence-Bond Solid in Two Dimensions: Evidence for Logarithmic Corrections to Scaling, Phys. Rev. Lett. **104**, 177201 (2010).

[43] A. W. Sandvik, V. N. Kotov, and O. P. Sushkov, Thermodynamics of a Gas of Deconfined Bosonic Spinons in two Dimensions, Phys. Rev. Lett. **106**, 207203 (2011).

[44] A. Nahum, J. T. Chalker, P. Serna, M. Ortuño, and A. M. Somoza, 3D Loop Models and the CP^{n-1} Sigma Model, Phys. Rev. Lett. **107**, 110601 (2011).

[45] L. Bartosch, Corrections to scaling in the critical theory of deconfined criticality, Phys. Rev. B **88**, 195140 (2013).

[46] F. S. Nogueira and A. Sudbø, Deconfined quantum criticality and conformal phase transition in two-dimensional antiferromagnets, Europhys. Lett. **104**, 56004 (2013).

[47] Y. Tang and A. W. Sandvik, Confinement and Deconfinement of Spinons in Two Dimensions, Phys. Rev. Lett. **110**, 217213 (2013).

[48] S. Pujari, F. Alet, and K. Damle, Transitions to valence-bond solid order in a honeycomb lattice antiferromagnet, Phys. Rev. B **91**, 104411 (2015).

[49] A. Nahum, J. T. Chalker, P. Serna, M. Ortuño, and A. M. Somoza, Deconfined Quantum Criticality, Scaling Violations, and Classical Loop Models, Phys. Rev. X **5**, 041048 (2015).

[50] H. Shao, W. Guo, and A. W. Sandvik, Quantum criticality with two length scales, Science **352**, 213 (2016).

[51] J. D'Emidio and R. K. Kaul, New Easy-Plane $\mathbb{C}\mathbb{P}^{N-1}$ Fixed Points, Phys. Rev. Lett. **118**, 187202 (2017).

[52] Y. Q. Qin, Y.-Y. He, Y.-Z. You, Z.-Y. Lu, A. Sen, A. W. Sandvik, C. Xu, and Z. Y. Meng, Duality between the Deconfined Quantum-Critical Point and the Bosonic Topological Transition, Phys. Rev. X **7**, 031052 (2017).

[53] C. Wang, A. Nahum, M. A. Metlitski, C. Xu, and T. Senthil, Deconfined Quantum Critical Points: Symmetries and Dualities, Phys. Rev. X **7**, 031051 (2017).

[54] H. Shao, Y. Q. Qin, S. Capponi, S. Chesi, Z. Y. Meng, and A. W. Sandvik, Nearly Deconfined Spinon Excitations in the Square-Lattice Spin-1/2 Heisenberg Antiferromagnet, Phys. Rev. X **7**, 041072 (2017).

[55] L. Janssen and Y.-C. He, Critical behavior of the QED_3-Gross-Neveu model: Duality and deconfined criticality, Phys. Rev. B **96**, 205113 (2017).

[56] Y.-Z. You, Y.-C. He, C. Xu, and A. Vishwanath, Symmetric Fermion Mass Generation as Deconfined Quantum Criticality, Phys. Rev. X **8**, 011026 (2018).

[57] A. Thomson and S. Sachdev, Fermionic Spinon Theory of Square Lattice Spin Liquids Near the Néel State, Phys. Rev. X **8**, 011012 (2018).

[58] X.-F. Zhang, Y.-C. He, S. Eggert, R. Moessner, and F. Pollmann, Continuous Easy-Plane Deconfined Phase Transition on the Kagome Lattice, Phys. Rev. Lett. **120**, 115702 (2018).

[59] C.-M. Jian, A. Thomson, A. Rasmussen, Z. Bi, and C. Xu, Deconfined quantum critical point on the triangular lattice, Phys. Rev. B **97**, 195115 (2018).

[60] S. Gazit, F. F. Assaad, S. Sachdev, A. Vishwanath, and C. Wang, Confinement transition of $\mathbb{Z}_2$ gauge theories coupled to massless fermions: Emergent quantum chromodynamics and SO(5) symmetry, Proc. Natl. Acad. Sci. USA **115**, E6987 (2018).

[61] Y. Liu, Z. Wang, T. Sato, M. Hohenadler, C. Wang, W. Guo, and F. F. Assaad, Superconductivity from the condensation of topological defects in a quantum spin-hall insulator, Nat. Commun. **10**, 2658 (2019).

[62] Z.-X. Li, S.-K. Jian, and H. Yao, Deconfined quantum criticality and emergent SO(5) symmetry in fermionic systems, arXiv:1904.10975.

[63] B. Ihrig, N. Zerf, P. Marquard, I. F. Herbut, and M. M. Scherer, Abelian Higgs model at four loops, fixed-point collision, and deconfined criticality, Phys. Rev. B **100**, 134507 (2019).

[64] L. Janssen, W. Wang, M. M. Scherer, Z. Y. Meng, and X. Y. Xu, Confinement transition in the QED_3-Gross-Neveu-XY universality class, Phys. Rev. B **101**, 235118 (2020).

[65] A. W. Sandvik and B. Zhao, Consistent scaling exponents at the deconfined quantum-critical point, Chin. Phys. Lett. **37**, 057502 (2020).

[66] M. E. Zayed, C. Rüegg, J. Larrea J., A. M. Läuchli, C. Panagopoulos, S. S. Saxena, M. Ellerby, D. F. McMorrow, T. Strässle, S. Klotz, G. Hamel, R. A. Sadykov, V. Pomjakushin, M. Boehm, M. Jiménez-Ruiz, A. Schneidewind, E. Pomjakushina, M. Stingaciu, K. Conder, and H. M. Rønnow, 4-spin plaquette singlet state in the Shastry-Sutherland compound SrCu2(BO3)2, Nat. Phys. **13**, 962 (2017).

[67] A. Nahum, P. Serna, J. T. Chalker, M. Ortuño, and A. M. Somoza, Emergent SO(5) Symmetry at the Néel to Valence-Bond-Solid Transition, Phys. Rev. Lett. **115**, 267203 (2015).

[68] G. J. Sreejith, S. Powell, and A. Nahum, Emergent SO(5) Symmetry at the Columnar Ordering Transition in the Classical Cubic Dimer Model, Phys. Rev. Lett. **122**, 080601 (2019).

[69] N. Ma, Y.-Z. You, and Z. Y. Meng, Role of Noether's Theorem at the Deconfined Quantum Critical Point, Phys. Rev. Lett. **122**, 175701 (2019).

[70] M. Oshikawa, Ordered phase and scaling in Z_n models and the three-state antiferromagnetic Potts model in three dimensions, Phys. Rev. B **61**, 3430 (2000).

[71] J. Lou, A. W. Sandvik, and L. Balents, Emergence of U(1) Symmetry in the 3D XY Model with Z_q Anisotropy, Phys. Rev. Lett. **99**, 207203 (2007).

[72] T. Okubo, K. Oshikawa, H. Watanabe, and N. Kawashima, Scaling relation for dangerously irrelevant symmetry-breaking fields, Phys. Rev. B **91**, 174417 (2015).

[73] H. Shao, W. Guo, and A. W. Sandvik, Monte Carlo Renormalization Flows in the Space of Relevant and Irrelevant Operators: Application to Three-Dimensional Clock Models, Phys. Rev. Lett. **124**, 080602 (2020).

[74] P. Patil, H. Shao, and A. W. Sandvik, Unconventional U(1) to Z_q crossover in quantum and classical q-state clock models, Phys. Rev. B **103**, 054418 (2021).

[75] F. Léonard and B. Delamotte, Critical Exponents can be Different on the Two Sides of a Transition: A Generic Mechanism, Phys. Rev. Lett. **115**, 200601 (2015).

[76] A. Kuklov, N. Prokof'ev, and B. Svistunov, Weak first-order superfluid-solid quantum transitions and deconfined criticality, Prog. Theor. Phys. Suppl. **160**, 337 (2005).

[77] A. Kuklov, N. Prokof'ev, B. Svistunov, and M. Troyer, Deconfined criticality, runaway flow in the two-component scalar electrodynamics and weak first-order superfluid-solid transitions, Ann. Phys. **321**, 1602 (2006).

[78] A. B. Kuklov, M. Matsumoto, N. V. Prokof'ev, B. V. Svistunov, and M. Troyer, Deconfined Criticality: Generic First-Order Transition in the SU(2) Symmetry Case, Phys. Rev. Lett. **101**, 050405 (2008).

[79] F.-J. Jiang, M. Nyfeler, S. Chandrasekharan, and U.-J. Wiese, From an antiferromagnet to a valence bond solid: Evidence for a first-order phase transition, J. Stat. Mech.: Theory Exp. (2008) P02009.

[80] K. Chen, Y. Huang, Y. Deng, A. B. Kuklov, N. V. Prokof'ev, and B. V. Svistunov, Deconfined Criticality Flow in the Heisenberg Model With Ring-Exchange Interactions, Phys. Rev. Lett. **110**, 185701 (2013).

[81] V. Gorbenko, S. Rychkov, and B. Zan, Walking, weak first-order transitions, and complex CFTs, J. High Energy Phys. 10 (2018) 108.

[82] V. Gorbenko, S. Rychkov, and B. Zan, Walking, Weak first-order transitions, and complex CFTs II. Two-dimensional Potts model at $Q > 4$, SciPost Phys. **5**, 050 (2018).

[83] R. Ma and C. Wang, Theory of deconfined pseudocriticality, Phys. Rev. B **102**, 020407(R) (2020).

[84] A. Nahum, Note on Wess-Zumino-Witten models and quasiuniversality in $2+1$ dimensions, Phys. Rev. B **102**, 201116(R) (2020).

[85] J. D'Emidio, A. A. Eberharter, and A. M. Läuchli, Diagnosing weakly first-order phase transitions by coupling to order parameters, arXiv:2106.15462.

[86] P. C. Hohenberg and B. I. Halperin, Theory of dynamic critical phenomena, Rev. Mod. Phys. **49**, 435 (1977).

[87] J. Dziarmaga, Dynamics of a quantum phase transition and relaxation to a steady state, Adv. Phys. **59**, 1063 (2010).

[88] A. Polkovnikov, K. Sengupta, A. Silva, and M. Vengalattore, Colloquium: Nonequilibrium dynamics of closed interacting quantum systems, Rev. Mod. Phys. **83**, 863 (2011).

[89] L. D'Alessio, Y. Kafri, A. Polkovnikov, and M. Rigol, From quantum chaos and eigenstate thermalization to statistical mechanics and thermodynamics, Adv. Phys. **65**, 239 (2016).

[90] A. Mitra, Quantum quench dynamics, Annu. Rev. Condens. Matter Phys. **9**, 245 (2018).

[91] H. K. Janssen, B. Schaub, and B. Schmittmann, New universal short-time scaling behaviour of critical relaxation processes, Z. Phys. B **73**, 539 (1989).

[92] Z. B. Li, L. Schülke, and B. Zheng, Dynamic Monte Carlo Measurement of Critical Exponents, Phys. Rev. Lett. **74**, 3396 (1995).

[93] B. Zheng, Generalized Dynamic Scaling for Critical Relaxations, Phys. Rev. Lett. **77**, 679 (1996).

[94] E. V. Albano, M. A. Bab, G. Baglietto, R. A. Borzi, T. S. Grigera, E. S. Loscar, D. E. Rodriguez, M. L. R. Puzzo, and G. P. Saracco, Study of phase transitions from short-time non-equilibrium behaviour, Rep. Prog. Phys. **74**, 026501 (2011).

[95] S. Yin, P. Mai, and F. Zhong, Universal short-time quantum critical dynamics in imaginary time, Phys. Rev. B **89**, 144115 (2014).

[96] S. Zhang, S. Yin, and F. Zhong, Generalized dynamic scaling for quantum critical relaxation in imaginary time, Phys. Rev. E **90**, 042104 (2014).

[97] Y.-R. Shu, S. Yin, and D.-X. Yao, Universal short-time quantum critical dynamics of finite-size systems, Phys. Rev. B **96**, 094304 (2017).

[98] Y.-R. Shu and S. Yin, Short-imaginary-time quantum critical dynamics in the $J - Q_3$ spin chain, Phys. Rev. B **102**, 104425 (2020).

[99] Z. Zuo, S. Yin, X. Cao, and F. Zhong, Scaling theory of the Kosterlitz-Thouless phase transition, Phys. Rev. B **104**, 214108 (2021).

[100] Y.-R. Shu, S.-K. Jian, and S. Yin, Nonequilibrium Dynamics of Deconfined Quantum Critical Point in Imaginary Time, Phys. Rev. Lett. **128**, 020601 (2022).

[101] Y. Tang and A. W. Sandvik, Method to Characterize Spinons as Emergent Elementary Particles, Phys. Rev. Lett. **107**, 157201 (2011).

[102] O. I. Motrunich and A. Vishwanath, Emergent photons and transitions in the O(3) sigma model with hedgehog suppression, Phys. Rev. B **70**, 075104 (2004).

[103] F. D. M. Haldane, O(3) Nonlinear σ Model and the Topological Distinction Between Integer- and Half-Integer-Spin Antiferromagnets in Two Dimensions, Phys. Rev. Lett. **61**, 1029 (1988).

[104] N. Read and S. Sachdev, Spin-Peierls, valence-bond solid, and Néel ground states of low-dimensional quantum antiferromagnets, Phys. Rev. B **42**, 4568 (1990).

[105] N. Read and S. Sachdev, Large- N Expansion for Frustrated Quantum Antiferromagnets, Phys. Rev. Lett. **66**, 1773 (1991).

[106] A. W. Sandvik, Computational studies of quantum spin systems, AIP Conf. Proc. **1297**, 135 (2010).

[107] C.-W. Liu, A. Polkovnikov, and A. W. Sandvik, Quasi-adiabatic quantum Monte Carlo algorithm for quantum evolution in imaginary time, Phys. Rev. B **87**, 174302 (2013).

[108] C. D. Grandi, A. Polkovnikov, and A. W. Sandvik, Microscopic theory of non-adiabatic response in real and imaginary time, J. Phys.: Condens. Matter **25**, 404216 (2013).

[109] E. Farhi, D. Gosset, I. Hen, A. W. Sandvik, P. Shor, A. P. Young, and F. Zamponi, Performance of the quantum adiabatic algorithm on random instances of two optimization problems on regular hypergraphs, Phys. Rev. A **86**, 052334 (2012).

[110] H. Shao, W. Guo, and A. W. Sandvik, Emergent topological excitations in a two-dimensional quantum spin system, Phys. Rev. B **91**, 094426 (2015).

[111] P. Weinberg and A. W. Sandvik, Dynamic scaling of the restoration of rotational symmetry in Heisenberg quantum antiferromagnets, Phys. Rev. B **96**, 054442 (2017).

[112] K. Beach and A. W. Sandvik, Some formal results for the valence bond basis, Nucl. Phys. B **750**, 142 (2006).

[113] A. W. Sandvik and H. G. Evertz, Loop updates for variational and projector quantum Monte Carlo simulations in the valence-bond basis, Phys. Rev. B **82**, 024407 (2010).

[114] S. Ferrara, R. Gatto, and A. Grillo, Positivity restriction on anomalous dimensions, Phys. Rev. D **9**, 3564 (1974).

[115] G. Mack, All unitary ray representations of the conformal group SU(2, 2) with positive energy, Commun. Math. Phys. **55**, 1 (1977).

[116] H. Suwa, A. Sen, and A. W. Sandvik, Level spectroscopy in a two-dimensional quantum magnet: Linearly dispersing spinons at the deconfined quantum critical point, Phys. Rev. B **94**, 144416 (2016).

[117] E. A. Martinez, C. A. Muschik, P. Schindler, D. Nigg, A. Erhard, M. Heyl, P. Hauke, M. Dalmonte, T. Monz, P. Zoller, and R. Blatt, Real-time dynamics of lattice gauge theories with a few-qubit quantum computer, Nature (London) **534**, 516 (2016).

[118] C. W. Bauer, B. Nachman, and M. Freytsis, Simulating Collider Physics on Quantum Computers Using Effective Field Theories, Phys. Rev. Lett. **127**, 212001 (2021).

[119] K. J. Satzinger, Y.-J. Liu, A. Smith, C. Knapp, M. Newman, C. Jones, Z. Chen, C. Quintana, X. Mi, A. Dunsworth, C. Gidney, I. Aleiner, F. Arute, K. Arya, J. Atalaya, R. Babbush, J. C. Bardin, R. Barends, J. Basso, A. Bengtsson *et al.*, Realizing topologically ordered states on a quantum processor, Science **374**, 1237 (2021).

[120] G. Semeghini, H. Levine, A. Keesling, S. Ebadi, T. T. Wang, D. Bluvstein, R. Verresen, H. Pichler, M. Kalinowski, R. Samajdar, A. Omran, S. Sachdev, A. Vishwanath, M. Greiner, V. Vuletić, and M. D. Lukin, Probing topological spin liquids on a programmable quantum simulator, Science **374**, 1242 (2021).

[121] P. Weinberg, M. Tylutki, J. M. Rönkkö, J. Westerholm, J. A. Åström, P. Manninen, P. Törmä, and A. W. Sandvik, Scaling and Diabatic Effects in Quantum Annealing with a D-Wave Device, Phys. Rev. Lett. **124**, 090502 (2020).

[122] M. Dupont and J. E. Moore, Quantum criticality using a superconducting quantum processor, arXiv:2109.10909.

[123] M. Motta, C. Sun, A. T. K. Tan, M. J. O'Rourke, E. Ye, A. J. Minnich, F. G. S. L. Brandão, and G. K.-L. Chan, Determining eigenstates and thermal states on a quantum computer using quantum imaginary time evolution, Nat. Phys. **16**, 205 (2020).

[124] H. Nishi, T. Kosugi, and Y.-i. Matsushita, Implementation of quantum imaginary-time evolution method on NISQ devices by introducing nonlocal approximation, npj Quantum Inf. **7**, 85 (2021).

[125] C. De Grandi, A. Polkovnikov, and A. W. Sandvik, Universal nonequilibrium quantum dynamics in imaginary time, Phys. Rev. B **84**, 224303 (2011).

[126] M. Kolodrubetz, D. Sels, P. Mehta, and A. Polkovnikov, Geometry and non-adiabatic response in quantum and classical systems, Phys. Rep. **697**, 1 (2017).

[127] E. G. Dalla Torre, E. Demler, and A. Polkovnikov, Universal Rephasing Dynamics After a Quantum Quench Via Sudden Coupling of Two Initially Independent Condensates, Phys. Rev. Lett. **110**, 090404 (2013).

[128] P. Gagel, P. P. Orth, and J. Schmalian, Universal Postquench Prethermalization at a Quantum Critical Point, Phys. Rev. Lett. **113**, 220401 (2014).

[129] A. Maraga, A. Chiocchetta, A. Mitra, and A. Gambassi, Aging and coarsening in isolated quantum systems after a quench: Exact results for the quantum O(N) model with $N \to \infty$, Phys. Rev. E **92**, 042151 (2015).

[130] A. Chiocchetta, M. Tavora, A. Gambassi, and A. Mitra, Short-time universal scaling in an isolated quantum system after a quench, Phys. Rev. B **91**, 220302(R) (2015).

[131] A. Chiocchetta, M. Tavora, A. Gambassi, and A. Mitra, Short-time universal scaling and light-cone dynamics after a quench in an isolated quantum system in d spatial dimensions, Phys. Rev. B **94**, 134311 (2016).

[132] A. Chiocchetta, A. Gambassi, S. Diehl, and J. Marino, Dynamical Crossovers in Prethermal Critical States, Phys. Rev. Lett. **118**, 135701 (2017).

[133] S.-K. Jian, S. Yin, and B. Swingle, Universal Prethermal Dynamics in Gross-Neveu-Yukawa Criticality, Phys. Rev. Lett. **123**, 170606 (2019).

[134] S. Yin and S.-K. Jian, Fermion-induced dynamical critical point, Phys. Rev. B **103**, 125116 (2021).

[135] J. C. Halimeh and M. F. Maghrebi, Quantum aging and dynamical universality in the long-range $O(N \to \infty)$ model, Phys. Rev. E **103**, 052142 (2021).